Prepared for submission to JHEP YACHAY-PUB-16-02-PN

A framework for testing leptonic unitarity by neutrino oscillation experiments

Chee Sheng Fong[1] **Hisakazu Minakata**[2] **Hiroshi Nunokawa**[3]

[1] *Instituto de Física, Universidade de São Paulo, C. P. 66.318, 05315-970 São Paulo, Brazil*
[2] *Department of Physics, Yachay Tech, San Miguel de Urcuquí, 100119 Ecuador*
[3] *Departamento de Física, Pontifícia Universidade Católica do Rio de Janeiro, C. P. 38097, 22451-900, Rio de Janeiro, Brazil*

E-mail: fong@if.usp.br, hminakata@yachaytech.edu.ec, nunokawa@puc-rio.br

Abstract: If leptonic unitarity is violated by new physics at an energy scale much lower than the electroweak scale, which we call low-scale unitarity violation, it has different characteristic features from those expected in unitarity violation at high-energy scales. They include maintaining flavor universality and absence of zero-distance flavor transition. We present a framework for testing such unitarity violation at low energies by neutrino oscillation experiments. Starting from the unitary 3 active plus N (arbitrary integer) sterile neutrino model we show that by restricting the active-sterile and sterile-sterile neutrino mass squared differences to $\gtrsim 0.1$ eV^2 the oscillation probability in the $(3+N)$ model becomes insensitive to details of the sterile sector, providing a nearly model-independent framework for testing low-scale unitarity violation. Yet, the presence of the sterile sector leaves trace as a constant probability leaking term, which distinguishes low-scale unitarity violation from the high-scale one. The non-unitary mixing matrix in the active neutrino subspace is common for the both cases. We analyze how severely the unitarity violation can be constrained in ν_e-row by taking a JUNO-like setting to simulate medium baseline reactor experiments. Possible modification of the features of the $(3+N)$ model due to matter effect is discussed to first order in the matter potential.

arXiv:1609.08623v1 [hep-ph] 27 Sep 2016

Contents

1 Introduction **2**

2 Unitarity violation at high- and low-energy scales **4**

3 A model of unitarity violation at low energies **5**
- 3.1 3 active $+N$ sterile unitary system 5
- 3.2 Averaging out the sterile oscillations due to decoherence 6
- 3.3 Requirement on the sterile mass spectrum 8
- 3.4 Cases in which sterile oscillations are not averaged out 8

4 The oscillation probabilities in 3 active and N sterile model in vacuum **9**
- 4.1 No zero distance transition in $(3+N)\times(3+N)$ unitary system 9
- 4.2 The oscillation probabilities in the $(3+N)$ model 9
- 4.3 $(3+N)$ state space unitarity and constraint on probability leaking term 12
- 4.4 Summarizing our method of testing leptonic unitarity 13

5 Unitarity violation in vacuum: Case study using JUNO-like setting **14**
- 5.1 Analysis method 14
- 5.2 Analysis result 15
  - 5.2.1 Comparison between the unitary and the non-unitarity cases 15
  - 5.2.2 Understanding correlations between the parameters 17

6 Structure of CP violation in the $(3+N)$ space unitary model **19**

7 Unitarity violation in matter: Matter perturbation theory **21**
- 7.1 Matter perturbation theory of three active plus N sterile unitary system 22
- 7.2 Perturbation theory in vacuum mass eigenstate basis 22
- 7.3 Disappearance channels 24
- 7.4 Appearance channels 26

8 Conclusions **27**

A Bounds on the probability leaking term by $(3+N)$ space unitarity **29**

B Comparison between the non-unitary constrained and constraint-free cases **30**

C $\tilde{S}$ matrix elements **32**

D Oscillation probabilities in the disappearance channels **33**

E Oscillation probabilities in the appearance channels **35**

F Number of events for the JUNO-like setting **38**

1 Introduction

Determination of leptonic mixing parameters, the three mixing angles and the two mass squared differences of neutrinos, marks a new epoch of physics beyond the standard model (SM). Despite that we still do not know the value of leptonic Kobayashi-Maskawa phase and the neutrino mass pattern, successes of *hypothesis* of using the standard three-flavor mixing in describing a wealth of experimental data prompts us to think about one further step, namely, the paradigm test. We feel that we have reached the right point that raising the question of how to test the three-flavor mixing framework itself is timely.

The most common way of testing the framework is to verify unitarity of the mixing matrix. It appears to us that the two different strategies of testing leptonic unitarity are thinkable:

- One is to show closing of the lepton unitarity triangle in an analogous way of unitarity test for the quark CKM matrix [1].
- The other is to prepare a model of unitarity violation, confront it against the available experimental data, and derive constraints on unitarity violation parameters.

The first method serves as a unitarity test purely within the framework of standard three-flavor mixing scheme of neutrinos, without recourse to any particular model of unitarity violation. This is the advantage of this method. See e.g., ref. [2] for this approach. In the second way, one introduces a general framework for leptonic unitarity violation, or a class of models that embody the property is constructed.

To our opinion, there are pros and cons in the above two different strategies. In the first method, despite its charming model-independent nature, it is quite challenging to determine size of each side of the unitarity triangles experimentally [2]. The second method introduces model-dependent features into the unitarity test, which can be considered as a drawback of this approach. On the other hand, there is a definite underlying scenario behind the non-unitarity in the latter case, or at least general guidance to it. Therefore, once hinted, it may allow us to identify the cause of unitarity violation. We feel, therefore, that both methods of leptonic unitarity test must be pursued.

In studies of testing leptonic unitarity so far done along the second strategy above, it appears that people took two different attitudes. That is, one integrates out new physics effects at high energy scales to obtain effective theories of three generation leptons at low energies which represents non-unitarity in this limited subspace [3]. The other one takes more relaxed attitude in explicitly introducing SM singlet leptons, and examines the models in a relatively model independent fashion in SM subspace with non-unitarity [4, 5]. In the latter approach, the masses of SM gauge-group singlet leptons can be large or small, reflecting varying underlying scenarios of new physics. If we take the former

way, $SU(2) \times U(1)$ gauge invariance dictates that the same unitarity violation must also be manifest in the charged lepton sector. In the framework of ref. [3], generally speaking, the constraints on unitarity violation are dominated by the ones coming from the charged lepton sector. If we follow the latter way, it is more case-sensitive and neutrino experiments can play greater roles. One of the most interesting questions in the whole area of study of unitarity violation is to reveal qualitative differences between unitarity violation at high- and low-energy scales.

It is the purpose of this paper to discuss low-energy scale unitarity violation, hereafter *"low-scale unitarity violation"* for short, in detail. By low-scale unitarity violation we mean that a "hidden" sector in state space to which probability flow occurs is located at low energy scales, like eV or MeV. It allows the hidden sector particles be produced along with neutrinos, and also they participate in neutrino oscillations assuming their mixing with neutrinos. We first recapitulate the interesting characteristic features of low-scale unitarity violation different from high-scale unitarity violation. They include (1) retaining flavor universality, and (2) lack of zero-distance flavor transitions. See section 2 for more about these points.

Then, we go on to construct a framework for experimental testing of low-scale unitarity violation. Since there is such interesting qualitative differences above between high- and low-scale unitarity violation, they must be tested and be distinguished from each other.[1] We argue, in agreement with the preceding works [4, 5], that the constraint by Z width measurement in LEP [10] makes extension of low-mass lepton sector to be essentially unique, only allowing inclusion of SM singlet fermions. Thus, our model of non-unitarity at low-energies utilizes three active neutrinos and an arbitrary numbers of sterile neutrino states.

We discuss in detail how the model prediction can be made insensitive to the details of the sterile sector, e.g., the mass spectrum of sterile neutrinos and mixing between active and sterile neutrinos. We find that the resultant expressions of oscillation probabilities in vacuum contain a new term, an explicit probability leakage term, which distinguishes between low- and high-scale unitarity violation. To our knowledge, the term has not been incorporated in the previous analyses of unitarity violation at low energies. We examine how this framework works by analyzing future medium-baseline reactor neutrino experiments. In the final two sections we discuss how CP violating terms in accelerator appearance measurement can be used to signal uni-unitarity and how the matter effect affects the foregoing discussions above.

There is an obvious relation between the model we discuss in this paper and various versions of active plus sterile neutrino models proposed to provide description of the LSND-MiniBooNE anomaly (see a review [11] and references therein). We will make remarks on the relationship between them below at wherever appropriate. In particular, we should note that in the frameworks of 3 active plus a few sterile neutrinos the various bounds on the mixing parameters are derived by using the existing data. For the most recent comprehensive analysis, see ref. [12].[2]

[1] Specific scenarios about high- and low-scale unitarity violation were explored in refs. [6–9].

[2] Though they are very relevant for this paper we do not implement these bounds into discussions in this

2 Unitarity violation at high- and low-energy scales

The cause of unitarity violation in the lepton sector can be due to new physics beyond the SM at high-energy scales, or the ones at low energies. In the best studied high-scale seesaw scenario of neutrino mass [13–16], the three-flavor mixing of neutrinos has a tiny violation of unitarity due to the mixing of heavy right-handed neutrinos. A more generic formulation of high-scale unitarity violation was given by Antusch et al. [3] by taking the minimal unitarity violation scheme. One of the salient features in high-scale unitarity violation is that even though SM singlet leptons exist which mix with neutrinos, it is likely that such neutral leptons are much heavier than neutrinos. They are not produced copiously in the same processes as neutrinos are produced, and a physical transition from neutrinos to them are kinematically forbidden.

On the other hand, if we assume that unitarity violation occurs due to physics at an energy scale much lower than the electroweak scale, the light SM gauge group singlet leptons not only mix with neutrinos, but also their masses are so light that they participate in the process of neutrino oscillations. In this paper, we try to develop a framework for experimental test of unitarity violation by assuming such situation, to which we simply refer as "low-scale unitarity violation". Hereafter, we call the SM gauge group singlet fermions generically as "sterile neutrinos" for simplicity.

We notice that there are some characteristic features in high- and low-scale unitarity violation that one can recognize even without going into any details. They are:

- Yes or no of violation of lepton universality: It is expected on general ground due to non-unitarity of the lepton mixing matrix the lepton universality is violated. See refs. [3, 4], and the references cited therein. While it is a generic feature in high-scale unitarity violation, lepton universality can be maintained in low-scale unitarity violation. It is because sterile neutrinos can be produced as well, for example in $\mu \to e +$ steriles process. Assuming no detector sensitivity to sterile neutrinos, it masks the effect of non-unitary mixing matrix in the active neutrino sector.

- Yes or no of zero distance neutrino flavor transition: Similarly to the above point, in high-scale unitarity violation, kinematically forbidden active to sterile states transition entails zero-distance attenuation of probability of a given flavor neutrino. It *does not* occur if sterile neutrinos can take part in the flavor oscillation processes, as we will show in section 4.1.

- Of course, there are common features in high- and low-scale unitarity violation: Emission of sterile neutrinos, if kinematically allowed range of low to high masses, affects the observable spectrum of charged leptons. It can be utilized to place constraints on non-unitarity by using, e.g., electron spectra in beta and muon decays, or muon spectrum in pion decay, cosmological observations etc. See [17] for a comprehensive summary of the current status of the bounds for the 3+1 scenario.

paper. It is because they are not derived by using the generic $(3 + N)$ model, and the translation of their bound to our setting requires great care. Furthermore, the principal purpose of this paper is to provide suitable framework for leptonic unitarity test in high-precision experiments in the future.

In the rest of this paper, we construct a model of low-scale unitarity violation which can be used to test leptonic unitarity in neutrino experiments. Although the constraints from beta and muon decays etc. just mentioned above are relevant, we do not try to elaborate the discussions already given in [17] and the references cited therein.

3 A model of unitarity violation at low energies

Now, we introduce our model of unitarity violation at low energies. But, one recognizes immediately that there is no big room for this. Precision measurement of Z decay width at LEP [10] dictates that there is only three active neutrinos. Therefore, extra fermions we introduce which mix with neutrinos must be SM singlets, which we call "sterile neutrinos" in this paper. Then, we are left with the unique possibility, the system of three active neutrinos plus arbitrary number of sterile neutrinos which mix with each other. We denote the number of sterile neutrino states as N. We assume that our system of the three active neutrinos and N sterile neutrinos are complete, which we call the $(3+N)$ **space unitary model** hereafter.

Though we deal with the particular model we want it as *model-independent* as possible within the framework of the $(3+N)$ space unitary model. Therefore, we shall always keep number of sterile neutrinos N arbitrary in this paper. Toward constructing a framework for leptonic unitarity test, however, we must make additional requirement on our $(3+N)$ space unitary model. We want to avoid the situation that experimental predictions of the model depend very sensitively on details of the N sterile neutrino sector, for example, on the mass spectrum of sterile states. In the rest of this section, we discuss how it can be achieved, and what are the conditions for this.

3.1 3 active $+N$ sterile unitary system

To define the notation and for definiteness, we introduce the $(3+N)$ space unitary system in vacuum. The Hamiltonian which governs the evolution of 3 active and N sterile state vector in flavor basis, $\nu = [\nu_e, \nu_\mu, \nu_\tau, s_1, s_2, \cdots, s_N]^T$, as $i\frac{d}{dx}\nu = H\nu$ is given by[3]

$$H = \mathbf{U} \begin{bmatrix} \Delta_1 & 0 & 0 & 0 & 0 & 0 \\ 0 & \Delta_2 & 0 & 0 & 0 & 0 \\ 0 & 0 & \Delta_3 & 0 & 0 & 0 \\ 0 & 0 & 0 & \Delta_4 & 0 & 0 \\ 0 & 0 & 0 & 0 & \cdots & 0 \\ 0 & 0 & 0 & 0 & 0 & \Delta_{3+N} \end{bmatrix} \mathbf{U}^\dagger \tag{3.1}$$

where

$$\Delta_i \equiv \frac{m_i^2}{2E} \quad (i = 1, 2, 3), \qquad \Delta_J \equiv \frac{m_J^2}{2E} \quad (J = 4, \cdots, 3+N). \tag{3.2}$$

[3] For simplicity, we assume that sterile states do not decay along its length of flight in neutrino oscillation experiments. If sterile states have decay length much shorter than the baseline, and if the decay products do not include the three active neutrinos, the oscillation probabilities converge to those of "high-scale unitarity violation" discussed in the previous section.

Here, m_i (m_J) denote the mass of mostly active (sterile) neutrinos and E is the neutrino energy.

For notations of the mass differences we use, in generic case including both active and sterile neutrinos,

$$\Delta m^2_{ab} \equiv m^2_a - m^2_b, \tag{3.3}$$

where $a, b = 1, ..., 3+N$. When we want to distinguish between active-active, active-sterile, and sterile-sterile neutrino mass differences, we use

$$\begin{aligned} \Delta m^2_{ji} &\equiv m^2_j - m^2_i, \\ \Delta m^2_{Ji} &\equiv m^2_J - m^2_i, \\ \Delta m^2_{JI} &\equiv m^2_J - m^2_I, \end{aligned} \tag{3.4}$$

where $i, j, k, ...$ (small letters) = 1,2,3 are for active neutrinos, and $I, J, K, ...$ (capital letters) = 4,.., 3+N for sterile neutrinos.

The mixing matrix $\mathbf{U}$ relates the flavor eigenstate ν to the vacuum mass eigenstate $\tilde{\nu}$ as $\nu_\alpha = \mathbf{U}_{\alpha a}\tilde{\nu}_a$ (here, $\alpha = e, \mu, \tau$), and hence it is a $(3+N) \times (3+N)$ matrix. By construction of the model, the matrix $\mathbf{U}$ is unitary.

3.2 Averaging out the sterile oscillations due to decoherence

How to make our model insensitive to the mass spectrum in the sterile sector? The masses of the sterile neutrinos appear in the factor of $e^{-iE_J x} = e^{-i\sqrt{p^2_J + m^2_J}x}$ in the propagations of mass eigenstates. This results in phase differences $e^{-i(E_J - E_I)x} \approx e^{-i\Delta m^2_{JI}x/(2E)}$ which can be observed through neutrino oscillation phenomena. Assuming no accidental mass degeneracy among the sterile states i.e. $|\Delta m^2_{JI}| \gg |\Delta m^2_{31}|$, the oscillation terms involving sterile masses can be averaged out due to (partial) decoherence if certain conditions are fulfilled.[4] Intuitively, decoherence occurs when the variation in the phase due to spatial and/or energy resolution is greater than 2π,

$$\left| \delta\left(\frac{\Delta m^2_{ab} x}{2E}\right) \right| = \left| \frac{\Delta m^2_{ab}}{2E}\delta x - \frac{\Delta m^2_{ab} x}{2E^2}\delta E \right| \gtrsim 2\pi. \tag{3.5}$$

From the terms in eq. (3.5) which depend, respectively, on the variation of baseline distance (δx) and that of energy (δE), we can classify the following two types of decoherence:

i. *Spatial resolution.* In this case, decoherence happens if

$$\delta x \gtrsim \frac{4\pi E}{|\Delta m^2_{ab}|}. \tag{3.6}$$

ii. *Energy resolution.* In this case, decoherence happens if

$$\delta E \gtrsim \frac{4\pi E^2}{|\Delta m^2_{ab}| x}. \tag{3.7}$$

[4] We are interested in partial decoherence where the oscillations involving sterile states are averaged out, whereas the active ones do oscillate.

Notice that the conditions derived heuristically above are in agreement with those obtained from formal approaches (i.e. wavepacket description) as e.g., in refs. [18–20]. Since we are interested in the decoherence involving sterile sector, the conditions (3.6) and (3.7) have to be fulfilled for Δm^2_{Ja} which involve at least one sterile mass. This allows us to obtain *lower* bound on the scale of sterile sector $|\Delta m^2_{Ja}|$ where our model becomes insensitive to the sterile mass spectrum. Notice that δx and δE in eqs. (3.6) and (3.7) are associated with the experimental setup (concerning *both* production and detection), e.g., with the production region of neutrinos and with energy resolution of a detector.

In the following, we discuss the conditions that must be satisfied for sterile oscillations to be averaged out. Most of the neutrino oscillation experiments work with the kinematical setting, either

$$\frac{\Delta m^2_{21} x}{4E} \sim 1 \qquad \text{or} \qquad \frac{|\Delta m^2_{31}| x}{4E} \sim 1. \tag{3.8}$$

in which the former is for long-baseline (LBL) reactor neutrino experiments, KamLAND, JUNO, and RENO-50, and the latter for the accelerator LBL and the reactor θ_{13} experiments.

From eq. (3.7), the condition for averaging out due to the size of production region, i.e. $\delta x = x_{\rm prod}$ reads

$$x_{\rm prod} \gtrsim \frac{4\pi E}{|\Delta m^2_{Ja}|}, \tag{3.9}$$

where $x_{\rm prod}$ denotes the size of the production region of neutrinos, e.g., core diameter for nuclear reactor neutrinos and the length of decay pipe for accelerator neutrino beams. Assuming the setting as in (3.8), the condition (3.9) leads to

$$\begin{aligned} |\Delta m^2_{Ja}| &\gtrsim \pi \Delta m^2_{21} \left(\frac{x}{x_{\rm prod}}\right) \approx 1.2\ {\rm eV}^2 \left(\frac{x/x_{\rm prod}}{5\times 10^3}\right) \qquad \text{(for reactor)}, \\ |\Delta m^2_{Ja}| &\gtrsim \pi |\Delta m^2_{31}| \left(\frac{x}{x_{\rm prod}}\right) \approx 7.5\ {\rm eV}^2 \left(\frac{x/x_{\rm prod}}{10^3}\right) \qquad \text{(for accelerator)}, \end{aligned} \tag{3.10}$$

where we have taken, for the typical source sizes and baseline distances, $x_{\rm prod} = 10$ m and $x = 50$ km for reactor neutrinos, and $x_{\rm prod} = 1$ km and $x = 1000$ km for accelerator neutrinos.

Due to energy resolution of a detector, using $\Delta m^2_{21} = 7.5\times 10^{-5}$ eV^2, and $|\Delta m^2_{31}| = 2.4\times 10^{-3}$ eV^2, eqs. (3.7) and (3.8) lead to the condition on Δm^2_{Ja} for the sterile oscillation to be averaged out:

$$\begin{aligned} |\Delta m^2_{Ja}| &\gtrsim \pi \left(\frac{\Delta m^2_{21}}{\delta E/E}\right) \approx 7.9\times 10^{-3}{\rm eV}^2 \left(\frac{\delta E/E}{0.03}\right)^{-1} \qquad \text{(for LBL reactor)}, \\ |\Delta m^2_{Ja}| &\gtrsim \pi \left(\frac{|\Delta m^2_{31}|}{\delta E/E}\right) \approx 7.5\times 10^{-2}{\rm eV}^2 \left(\frac{\delta E/E}{0.1}\right)^{-1} \qquad \text{(for accelerator)}. \end{aligned} \tag{3.11}$$

The aggressive choice of a typical 3% error in energy measurement in the former case is based on the JUNO proposal in [21], whereas a conservative choice of $\delta E/E = 10\%$ is

made for accelerator neutrino experiments. Therefore, if we restrict ourselves to $\Delta m^2_{Ji} \sim |\Delta m^2_{JK}| \gtrsim 0.1$ eV^2, the fast oscillation due to the active-sterile and sterile-sterile mass squared differences can be averaged out by the effect of energy resolution. For the JUNO-like setting the requirement on $|\Delta m^2_{Ja}|$ can be relaxed by an order of magnitude.

We note that effect of averaging over the production points of neutrinos is less sizeable compared to that of energy resolution for the fast sterile oscillation to be averaged out, which therefore leads to more restrictive condition on the sterile state masses.

3.3 Requirement on the sterile mass spectrum

In addition to the condition of averaging out the fast sterile oscillations, we require that the masses of sterile neutrinos are light enough such that they can be produced in the same environment as neutrinos are produced. We do this because it is the most significant characteristic feature of unitarity violation at low energies. It gives raise to the condition $m_J \lesssim 1$ MeV for reactor neutrinos, and $m_J \lesssim 100$ MeV for accelerator neutrinos.

To summarize: In seeking the case that neutrino oscillation in our 3 active + N sterile neutrino system is insensitive to the detailed properties of the sterile sector, such as spectrum of the sterile states and the fine structure of the active-sterile mixing, we require for sterile neutrino masses in our $(3+N)$ space unitary model that

$$0.1 \text{ eV}^2 \lesssim m^2_J \lesssim 1 \text{ MeV}^2. \tag{3.12}$$

The lower limit is from condition of averaging out the fast oscillations for accelerator neutrinos, and the upper one from producibility of sterile neutrinos in reactors.

With the conditions (3.6) and/or (3.7) of averaging out the fast oscillations being satisfied we can make approximation[5]

$$\left\langle \sin\left(\frac{\Delta m^2_{Ji} x}{2E}\right)\right\rangle \approx \left\langle \sin\left(\frac{\Delta m^2_{JK} x}{2E}\right)\right\rangle \approx 0, \tag{3.13}$$

$$\left\langle \cos\left(\frac{\Delta m^2_{Ji} x}{2E}\right)\right\rangle \approx \left\langle \cos\left(\frac{\Delta m^2_{JK} x}{2E}\right)\right\rangle \approx 0, \tag{3.14}$$

where $\langle ... \rangle$ stands for averaging over neutrino energy within the uncertainty of energy resolution, as well as averaging over uncertainty of distance between production and detection points of neutrinos. The latter approximate equalities in (3.13) and (3.14) assume that there is no accidental degeneracy among the sterile state masses i.e. $|\Delta m^2_{JK}| \gg |\Delta m^2_{31}|$.

3.4 Cases in which sterile oscillations are not averaged out

While allowing wide range of sterile lepton masses, the condition (3.12) excludes the certain characteristic regions of sterile neutrino mass spectrum. Exclusion of higher masses is done under the spirit of low-scale unitarity violation, and therefore we consider it granted. But, there is no a priori reason for excluding sterile neutrino masses in regions $\Delta m^2_{Ji} \sim |\Delta m^2_{JK}| \sim$ the atmospheric Δm^2, or the solar Δm^2. In this case, however, one must expect severe model dependence in the experimental predictions by the $(3+N)$ unitary model.

[5] To describe the borderline regime, one has to resort to formal description e.g. of refs. [18–20].

Clearly, the number of CP violating phases depends on N, and the additional phases will play important roles in fitting data. Therefore, an extensive separate treatment is necessary to include this case.

How about sterile neutrino masses which are much lighter than the atmospheric, or the solar Δm^2? Again, there is no a priori model-independent reason for excluding this case. If the active neutrino masses are such that KATRIN can detect the signal, $m_i \gtrsim 0.2$ eV, then, averaging out condition may be barely maintained for the fast active-sterile oscillation for very small sterile masses, $\Delta m^2 \simeq 0.04\,\text{eV}^2$. However, it would be accompanied by extremely slow developing (as a function of propagation distance x) sterile-sterile oscillations. Clearly, a separate analysis is needed to know to what extent the case survives a test with the currently available experimental data.

As a summary of our discussions in this section, we state as follows: If we construct $(3+N)$ space unitary system as a model of low-scale unitarity violation, we can make the model predictions insensitive to details of the sterile neutrino sector, such as the mass spectrum. It requires us to restrict ourselves to the region of sterile neutrino masses $0.1\ \text{eV}^2 \lesssim m_J^2 \lesssim 1\ \text{MeV}^2$. We assume this in our all subsequent discussions in this paper.

4 The oscillation probabilities in 3 active and N sterile model in vacuum

Given the Hamiltonian in (3.1), it is straightforward to compute the neutrino oscillation probabilities $P(\nu_\beta \to \nu_\alpha)$ in vacuum, where the Greek indices $\alpha, \beta, ... = e, \mu, \tau$. Let us start by showing that there is no zero distance transition in our $(3+N)$ space unitary model.

4.1 No zero distance transition in $(3+N)\times(3+N)$ unitary system

The oscillation probabilities take the form

$$\begin{aligned} P(\nu_\beta \to \nu_\alpha) &= \left| \sum_a \mathbf{U}_{\alpha a}\mathbf{U}^*_{\beta a}\, e^{-i\frac{m_a^2 x}{2E}} \right|^2 \\ &= \left| \sum_{a=1}^{3+N} \mathbf{U}_{\alpha a}\mathbf{U}^*_{\beta a} \right|^2 - 2\sum_{b\neq a} \text{Re}[\mathbf{U}_{\alpha a}\mathbf{U}^*_{\beta a}\mathbf{U}^*_{\alpha b}\mathbf{U}_{\beta b}] \sin^2\left(\frac{\Delta m^2_{ba}x}{4E}\right) \\ &\quad - \sum_{b\neq a} \text{Im}[\mathbf{U}_{\alpha a}\mathbf{U}^*_{\beta a}\mathbf{U}^*_{\alpha b}\mathbf{U}_{\beta b}] \sin\left(\frac{\Delta m^2_{ba}x}{2E}\right). \end{aligned} \tag{4.1}$$

At $x = 0$, $P(\nu_\beta \to \nu_\alpha) = \delta_{\alpha\beta}$ thanks to unitarity of the $\mathbf{U}$ matrix. It means, of course, no zero distance transition in the $(3+N)$ space unitary model. This is in sharp contrast to the feature possessed by the high-scale unitarity violation [3, 4].

4.2 The oscillation probabilities in the $(3+N)$ model

Here, we derive the expressions of the oscillation probabilities in our $(3+N)$ model when the active-sterile and sterile-sterile oscillations are averaged out. For this purpose we define a new notation of the $(3+N)\times(3+N)$ unitary matrix $\mathbf{U}$. It can be parameterized as [4]

$$\mathbf{U} = \begin{bmatrix} U & W \\ Z & V \end{bmatrix}, \tag{4.2}$$

satisfying $\mathbf{U}\mathbf{U}^\dagger = \mathbf{U}^\dagger\mathbf{U} = 1_{(3+N)\times(3+N)}$. The active space mixing matrix U is 3×3 matrix with elements $U_{\alpha i}$, the rectangular matrices W and Z are respectively $3\times N$ and $N\times 3$ matrices with elements $W_{\alpha I}$ and $Z_{I\alpha}$, and the square matrix V is $N\times N$ matrix with elements V_{IJ}. To develop general framework we do not make any assumptions on the size of W and Z matrix elements (besides $|W|, |Z| < 1$) in this paper.

The oscillation probability is written in terms of S matrix as $P(\nu_\beta \to \nu_\alpha) = |S_{\alpha\beta}|^2$,

$$S_{\alpha\beta} = \sum_{k=1}^{3} U_{\alpha k} U^*_{\beta k} e^{-i\Delta_k x} + \sum_{K=4}^{3+N} W_{\alpha K} W^*_{\beta K} e^{-i\Delta_K x}. \tag{4.3}$$

where $\Delta_{k(K)} \equiv m^2_{k(K)}/(2E)$ as defined in (3.2), and the elements of $3\times N$ matrix $\mathbf{W}$ are defined as

$$\mathbf{W} \equiv \begin{bmatrix} W_{e\,4} & W_{e\,5} & \dots & W_{e\,3+N} \\ W_{\mu\,4} & W_{\mu\,5} & \dots & W_{\mu\,3+N} \\ W_{\tau\,4} & W_{\tau\,5} & \dots & W_{\tau\,3+N} \end{bmatrix}, \tag{4.4}$$

such that its integer index indicated by the capital letters like I, J and K (which run from 4 to $3+N$) always refers to the sterile neutrino mass eigenstate.

After squaring the S matrix, $P(\nu_\beta \to \nu_\alpha)$ has three terms: the first and second terms squared and the interference term, each of which can be easily computed. They are given, in order, as

$$\begin{aligned} P(\nu_\beta \to \nu_\alpha) &= \left| \sum_{k=1}^{3} U_{\alpha k} U^*_{\beta k} \right|^2 \\ &- 2\sum_{j\neq k} \mathrm{Re}\left(U^*_{\alpha j} U_{\beta j} U_{\alpha k} U^*_{\beta k}\right) \sin^2 \frac{(\Delta_k - \Delta_j)x}{2} + \sum_{j\neq k} \mathrm{Im}\left(U^*_{\alpha j} U_{\beta j} U_{\alpha k} U^*_{\beta k}\right) \sin(\Delta_k - \Delta_j)x \\ &+ \sum_J |W_{\alpha J}|^2 |W_{\beta J}|^2 \\ &+ \sum_{J\neq K} \left[\mathrm{Re}\left(W^*_{\alpha J} W_{\beta J} W_{\alpha K} W^*_{\beta K}\right) \cos(\Delta_K - \Delta_J)x + \mathrm{Im}\left(W^*_{\alpha J} W_{\beta J} W_{\alpha K} W^*_{\beta K}\right) \sin(\Delta_K - \Delta_J)x\right] \\ &+ 2\sum_{j=1}^{3}\sum_{K=4}^{3+N} \left[\mathrm{Re}\left(U^*_{\alpha j} U_{\beta j} W_{\alpha K} W^*_{\beta K}\right) \cos(\Delta_K - \Delta_j)x + \mathrm{Im}\left(U^*_{\alpha j} U_{\beta j} W_{\alpha K} W^*_{\beta K}\right) \sin(\Delta_K - \Delta_j)x\right]. \end{aligned} \tag{4.5}$$

We notice that the last two lines vanish after averaging over energy resolution, as discussed in section 3. Then, we obtain the expressions of oscillation probabilities in our $(3+N)$ model in vacuum. In the appearance channel, $\alpha \neq \beta$, it reads

$$\begin{aligned} P(\nu_\beta \to \nu_\alpha) = \mathcal{C}_{\alpha\beta} &+ \left| \sum_{j=1}^{3} U_{\alpha j} U^*_{\beta j} \right|^2 - 2\sum_{j\neq k} \mathrm{Re}\left(U_{\alpha j} U^*_{\beta j} U^*_{\alpha k} U_{\beta k}\right) \sin^2 \frac{(\Delta_k - \Delta_j)x}{2} \\ &- \sum_{j\neq k} \mathrm{Im}\left(U_{\alpha j} U^*_{\beta j} U^*_{\alpha k} U_{\beta k}\right) \sin(\Delta_k - \Delta_j)x, \end{aligned} \tag{4.6}$$

and in the disappearance channel

$$P(\nu_\alpha \to \nu_\alpha) = \mathcal{C}_{\alpha\alpha} + \left(\sum_j^3 |U_{\alpha j}|^2\right)^2 - 4\sum_{k>j}^3 |U_{\alpha j}|^2 |U_{\alpha k}|^2 \sin^2 \frac{(\Delta_k - \Delta_j)x}{2}, \tag{4.7}$$

where[6]

$$\mathcal{C}_{\alpha\beta} \equiv \sum_{J=4}^{3+N} |W_{\alpha J}|^2 |W_{\beta J}|^2, \qquad \mathcal{C}_{\alpha\alpha} \equiv \sum_{J=4}^{3+N} |W_{\alpha J}|^4. \tag{4.8}$$

One should notice that after averaging over high-frequency sterile oscillations, the expressions in (4.6) and (4.7) have terms which look like the "zero-distance flavor transition". But, it cannot be the correct interpretation because the averaging procedure (even though it is on energy spectrum) inherently contains certain distance scale to observe destructive interference which leads to cancellation of oscillatory behavior.

The expression of the oscillation probabilities in (4.6) and (4.7) look similar to the ones in the standard three-flavor mixing. But, there are two important differences:

- The active space mixing matrix U is not unitary,
- There is a probability leaking term to the sterile neutrino sector, $\mathcal{C}_{\alpha\beta}$ in (4.6) and $\mathcal{C}_{\alpha\alpha}$ in (4.7).

The former is a common feature of the theories in which unitarity is violated in active neutrino subspace. In the unitary case the second term in (4.6) is $\delta_{\alpha\beta}$. On the other hand, the second point above, the existence of probability leaking term, is the characteristic feature of the low-scale unitarity violation. However, the term is omitted in the expression of the oscillation probability in the literature, e.g., in refs. [5, 23].

Does the leaking term introduce a heavy model-dependence into the prediction by our $(3+N)$ model? The answer is no: though it indeed displays some sterile sector model dependence, it is only a mild one. That is, the term can be treated as the channel dependent constant $\mathcal{C}_{\alpha\beta}$ when this formula is used to analyze leptonic unitarity violation in vacuum.

We emphasize that the clearest evidence for low-scale unitarity violation is the demonstration of existence of probability leaking constant $\mathcal{C}_{\alpha\beta} \equiv \sum_{J=4}^{3+N} |W_{\alpha J}|^2 |W_{\beta J}|^2$. Unfortunately, it would not be easy to carry out for the two reasons: (1) the term is small in size because it is the fourth order in unitarity-violating elements $W_{\alpha J}$, and (2) it is just a constant term and hence it could be confused by the uncertainty in the flux normalization of neutrino beams.

Apart from the probability leaking term $\mathcal{C}_{\alpha\beta}$ ($\alpha = \beta$, $\alpha \neq \beta$), our formulas agree with those of ref. [4]. On the other hand, the oscillation probability formulas in ref. [3] have extra normalization factor. Therefore, it looks like they do not agree with each other although they are both dealing with high-scale unitarity violation. But, since the normalization factor cancels against those included in the neutrino cross sections they are consistent, if the probability formulas in [4] are understood as the ones after the cancellation.

[6] The expression of $\mathcal{C}_{\alpha\alpha}$ was known but within the context of 3 active + 3 sterile model [22].

4.3 $(3+N)$ state space unitarity and constraint on probability leaking term

In our three active plus N sterile neutrino model, unitarity is obeyed in the whole $(3+N)$ state space, $\mathbf{U}\mathbf{U}^\dagger = \mathbf{U}^\dagger\mathbf{U} = \mathbf{1}$. It takes the form in the active 3×3 subspace

$$UU^\dagger + WW^\dagger = 1_{3\times 3}, \qquad U^\dagger U + Z^\dagger Z = 1_{3\times 3}. \tag{4.9}$$

The first relation in (4.9) implies that size of the probability leaking terms, $\mathcal{C}_{\alpha\beta}$ or $\mathcal{C}_{\alpha\alpha}$, and the size of unitarity violation in active space U matrix are related with each other.

In fact, it is easy to derive the upper and lower bounds on $\mathcal{C}_{\alpha\beta} = \sum_{J=4}^{3+N} |W_{\alpha J}|^2 |W_{\beta J}|^2$ and $\mathcal{C}_{\alpha\alpha} = \sum_{J=4}^{3+N} |W_{\alpha J}|^4$. One can start from

$$\left(\sum_I |W_{\alpha I}|^2\right)\left(\sum_J |W_{\beta J}|^2\right) = \sum_J |W_{\alpha J}|^2 |W_{\beta J}|^2 + \sum_{I\neq J} |W_{\alpha I}|^2 |W_{\beta J}|^2,$$
$$\left(\sum_J |W_{\alpha J}|^2\right)^2 = \sum_{J=1}^{N} |W_{\alpha J}|^4 + \sum_{I\neq J} |W_{\alpha I}|^2 |W_{\alpha J}|^2. \tag{4.10}$$

Since the last terms are non-negative we obtain the upper bounds[7]

$$\mathcal{C}_{\alpha\beta} \leq \left(1 - \sum_{j=1}^{3} |U_{\alpha j}|^2\right)\left(1 - \sum_{j=1}^{3} |U_{\beta j}|^2\right) \qquad (\alpha \neq \beta),$$
$$\mathcal{C}_{\alpha\alpha} \leq \left(1 - \sum_{j=1}^{3} |U_{\alpha j}|^2\right)^2. \tag{4.11}$$

The lower bound is slightly nontrivial, but they are derived in appendix A:

$$\mathcal{C}_{\alpha\beta} \geq \frac{1}{N}\left(1 - \sum_{j=1}^{3} |U_{\alpha j}|^2\right)\left(1 - \sum_{j=1}^{3} |U_{\beta j}|^2\right),$$
$$\mathcal{C}_{\alpha\alpha} \geq \frac{1}{N}\left(1 - \sum_{j=1}^{3} |U_{\alpha j}|^2\right)^2. \tag{4.12}$$

The lower bounds depend on N, and therefore they are sterile-sector model dependent. But, since the upper bounds are more restrictive, as we will see in the analysis in section 5, we assume the least conservative case, $N = \infty$ there.

Using (4.11) and (4.12), and the fact that $(1 - \sum_{i=1}^{3} |U_{\alpha i}|^2)$ and $\mathcal{C}_{\alpha\beta}$ are both positive, one can derive the bound $\sqrt{\mathcal{C}_{\alpha\beta}} \leq (1 - \sum_{i=1}^{3} |U_{\alpha i}|^2) \leq \sqrt{N\mathcal{C}_{\alpha\beta}}$. Suppose that the analysis of future experimental data indicates unitarity violation with nonzero value of $\mathcal{C}_{\alpha\beta}$ and $(1 - \sum_{i=1}^{3} |U_{\alpha i}|^2)$. If the data shows $(1 - \sum_{i=1}^{3} |U_{\alpha i}|^2) = \sqrt{M\mathcal{C}_{\alpha\beta}}$. Then, the $(3+N)$ space unitary model with $N < M$ is excluded.

[7] As pointed out in ref. [5], for $\alpha \neq \beta$ and $i \neq j$ cases respectively, there are two relevant bounds that can be obtained by applying Cauchy-Schwartz inequalities to unitarity constraints (4.9): $|\sum_{i=1}^{3} U_{\alpha i} U_{\beta i}^*|^2 \leq \left(1 - \sum_{j=1}^{3} |U_{\alpha j}|^2\right)\left(1 - \sum_{j=1}^{3} |U_{\beta j}|^2\right)$ and $|\sum_{\alpha=e}^{\tau} U_{\alpha i} U_{\alpha j}^*|^2 \leq \left(1 - \sum_{\alpha=e}^{\tau} |U_{\alpha i}|^2\right)\left(1 - \sum_{\alpha=e}^{\tau} |U_{\alpha j}|^2\right)$. These bounds are relevant when studying neutrino appearance $\nu_\alpha \to \nu_\beta$.

4.4 Summarizing our method of testing leptonic unitarity

Now, we can summarize our method of testing our $(3+N)$ model of low-scale unitarity violation in vacuum:

We fit the data by using the two ansatz: (1) the standard three-flavor mixing with unitary mixing matrix $U_{\rm PDG}$ [1], and (2) the expressions of the oscillation probabilities in (4.6) and (4.7), with the non-unitary U matrix and the probability leaking terms $\mathcal{C}_{\alpha\beta}$ and/or $\mathcal{C}_{\alpha\alpha}$. In the latter fit, it is important to place the constraints (4.11) on $\mathcal{C}_{\alpha\beta}$ and $\mathcal{C}_{\alpha\alpha}$. In section 5 we present an analysis of simulated JUNO data within our formalism.

One can think of various features of the fit results that can be obtained in this way. To discuss possible implications, let us assume for conceptual clarity that a set of super-high precision measurement were done by experiments with perfectly controlled neutrino beam.

- If the fit results using (1) the standard three-flavor mixing, and (2) the $(3+N)$ model reveal only small difference between them, it is an indication of absence of unitarity violation. One can obtain quantitative bounds on how severely unitarity violation is constrained.

- If the fit revealed a discrepancy between (1) and (2), it is an indication of unitarity violation. It is likely that the first indication of unitarity violation comes from nonzero values of $1-\sum_{i=1}^{3}|U_{\alpha i}|^2$ $(\alpha=e,\mu,\tau)$ in the disappearance channels, and/or $\left|\sum_{j=1}^{3}U_{\alpha j}U_{\beta j}^{*}\right|$ in the appearance channels. They are both of the order of W^2.

- If the measurement is sufficiently accurate to detect nonzero values of $\mathcal{C}_{\alpha\beta}$ $(\alpha\neq\beta$ and/or $\alpha=\beta)$ of the order of W^4, in addition to nonzero $1-\sum_{i=1}^{3}|U_{\alpha i}|^2$ and/or $\left|\sum_{j=1}^{3}U_{\alpha j}U_{\beta j}^{*}\right|$, it is a hint for low-scale unitarity violation.

- If the fit revealed a discrepancy between (1) and (2), indicating unitarity violation, and the fit results of $\mathcal{C}_{\alpha\beta}$ $(\alpha\neq\beta$ and/or $\alpha=\beta)$ is outside the region allowed by the constraints (4.11). Nonvanishing $\mathcal{C}_{\alpha\beta}$ suggests unitarity violation at low energies, which however implies that either both the conditions (3.6) and (3.7) are not satisfied or the scenario cannot be described by our $(3+N)$ space unitary model.

The final consistency check for proving low-scale unitarity violation in the third case above is to verify (i) the consistency between the magnitudes of $\mathcal{C}_{\alpha\beta}$ $(\sim W^4)$ and $1-\sum_{i=1}^{3}|U_{\alpha i}|^2$ and/or $\left|\sum_{j=1}^{3}U_{\alpha j}U_{\beta j}^{*}\right|$ $(\sim W^2)$, and (ii) over-all consistency between deviation of unitarity of U matrix and the size of W matrix expected from the $(3+N)$ space unitarity (4.9). We note that the relative magnitudes of $\mathcal{C}_{\alpha\beta}$ and $1-\sum_{i=1}^{3}|U_{\alpha i}|^2$ (or $\left|\sum_{j=1}^{3}U_{\alpha j}U_{\beta j}^{*}\right|$) is also enforced by the upper and lower bounds (4.11) and (4.12), and therefore the property is in the heart of the $(3+N)$ space unitary model.

A clarifying remark is in order: In the appearance oscillation probability, (4.6), $\left|\sum_{j=1}^{3}U_{\alpha j}U_{\beta j}^{*}\right|$ comes in as squared and the term is of the same order $\sim W^4$ as the leaking term $\mathcal{C}_{\alpha\beta}$. Therefore, one might think that the better accuracy may not be expected for $\left|\sum_{j=1}^{3}U_{\alpha j}U_{\beta j}^{*}\right|$.

The statement above that "$\left|\sum_{j=1}^{3} U_{\alpha j} U_{\beta j}^{*}\right|$ is the first indication of unitarity violation" really means that the non-unitary U matrix elements are determined mostly by the x/E dependent oscillation terms and it determines (or strongly constrains) $\left|\sum_{j=1}^{3} U_{\alpha j} U_{\beta j}^{*}\right|$, and in this way a better accuracy is expected for $\left|\sum_{j=1}^{3} U_{\alpha j} U_{\beta j}^{*}\right|$. The similar statement for disappearance channel also follows.

5 Unitarity violation in vacuum: Case study using JUNO-like setting

In this section we carry out the first test of our framework describing low-scale unitarity violation by applying it to data to be obtained by medium-baseline reactor neutrino experiments. For definiteness we assume the JUNO-like setting as defined below.[8]

We give special attention to the probability leaking term $\mathcal{C}_{\alpha\alpha}$ in eq. (4.7), as discussed in section 4.4. Of course, estimation of JUNO's capability of constraining (or probing) non-unitary nature of active space U matrix in the ν_e sector is a very interesting point by itself. Yet, we must admit that our analysis using a simple-minded χ^2 cannot be considered as the real quantitative one. We use the expression of disappearance probability $P(\nu_\alpha \to \nu_\alpha)$ ($\alpha = e$) in eq. (4.7) for reactor neutrino analysis because it is identical to $P(\bar{\nu}_\alpha \to \bar{\nu}_\alpha)$ assuming CPT invariance.

5.1 Analysis method

We basically follow the analysis done in [24] with some modification and simplification. In our statistical analysis, we define the χ^2 function which consists of two terms as,

$$\chi^2 \equiv \chi^2_{\rm stat} + \chi^2_{\rm sys}. \tag{5.1}$$

In the present analysis we do not take into account any data except for JUNO, not even precision measurement of $\sin^2\theta_{13}$ by Daya Bay and RENO [25, 26], which is expected to be improved to $\sim 3\%$ level. On this point, we will make a comment in section 5.2.

Following [27, 28], the $\chi^2_{\rm stat}$ is defined as,

$$\chi^2_{\rm stat} \equiv \int_0^{E_{\rm vis}^{\rm max}} dE_{\rm vis} \left(\frac{\dfrac{dN^{\rm obs}}{dE_{\rm vis}} - f_{\rm norm} \displaystyle\sum_{i={\rm reac}} \dfrac{dN_i^{\rm fit}}{dE_{\rm vis}}}{\sqrt{\dfrac{dN^{\rm obs}}{dE_{\rm vis}}}} \right)^2, \tag{5.2}$$

where $dN^{\rm obs}/dE_{\rm vis}$ denotes the energy distributions of the observed (simulated) signal, and $f_{\rm norm}$ is the flux normalization parameter for reactor neutrinos, to be varied freely subject to the pull term in $\chi^2_{\rm sys}$ (see below) and we integrate up to $E_{\rm vis}^{\rm max} = 8$ MeV. Due to the lack of space, we do not describe here how to compute the event number distribution $dN^{\rm obs}/dE_{\rm vis}$, leaving it to appendix F.

[8] The similar analysis of simulated JUNO data in the context of leptonic unitarity test was carried out in ref. [23]. See also section 3.3 of [21].

We consider only one kind of systematic error to take into account the reactor neutrino flux uncertainty,

$$\chi^2_{\rm sys} \equiv \left(\frac{1 - f_{\rm norm}}{\sigma_{f_{\rm norm}}} \right)^2 , \tag{5.3}$$

with $\sigma_{f_{\rm norm}} = 3\%$.

There are five relevant free parameters to be fitted in our analysis, namely, $|U_{e1}|^2$, $|U_{e2}|^2$, $\sum_{i=1}^3 |U_{ei}|^2$, $\mathcal{C}_{ee}$ as well as the flux normalization parameter, $f_{\rm norm}$. These five parameters are varied freely under the conditions,

$$\sum_{i=1}^{3} |U_{ei}|^2 \leq 1, \qquad 0 \leq \mathcal{C}_{ee} \leq (1 - \sum_{i=1}^{3} |U_{ei}|^2)^2, \tag{5.4}$$

as well as with the $\chi^2_{\rm sys}$ defined in (5.3). For simplicity, we fix the two mass squared differences as $\Delta m^2_{21} = 7.5 \times 10^{-5}$ eV^2, $\Delta m^2_{31} = 2.46 \times 10^{-3}$ eV^2 and consider only the case of normal mass hierarchy. We believe that even if we vary them our results would not change significantly.

Using the χ^2 function, we will determine the allowed ranges of the five parameters mentioned above, which will be projected into two or one dimensional subspace (see figure. 1 and table 1.) by using the conditions,

$$\Delta\chi^2 \equiv \chi^2 - \chi^2_{\rm min} = 2.3,\ 6.18 \text{ and } 11.93\ (1,\ 4 \text{ and } 9), \tag{5.5}$$

at 1, 2 and 3 σ CL, respectively, for two (one) degrees of freedom. Since we consider the input which corresponds the case without unitarity violation, $\chi^2_{\rm min} = 0$ by construction as we do not take into account the statistical fluctuation in simulating the artificial data.

5.2 Analysis result

In this section we present the results of our analysis of simulated JUNO data with particular emphasis to the bounds on the parameters, $\mathcal{C}_{ee}$ and $1 - \sum_{i=1}^3 |U_{ei}|^2$. A nonzero value of $\mathcal{C}_{ee}$ implies existence of the low-scale unitarity violation, distinguishing it from the high-scale unitarity violation. Unfortunately, size of $\mathcal{C}_{ee}$ is quite small because it is of the order of W^4. While the latter, $1 - \sum_{i=1}^3 |U_{ei}|^2$, being of the order of W^2, must be the first indicator of unitarity violation. We generate the input data without considering unitarity violation (corresponding to the standard three flavor scheme) but in the fit, we allow non-unitarity, in order to determine to what extent a JUNO-like experiment can constrain non-unitarity when the data are consistent with the standard three flavor scenario.

5.2.1 Comparison between the unitary and the non-unitarity cases

In figure 1 presented are the allowed regions of $\mathcal{C}_{ee}$, $\sum_{i=1}^3 |U_{ei}|^2$, $|U_{ei}|^2$ $(i = 1, 2)$, and the flux normalization $f_{\rm norm}$ projected onto the various two-dimensional spaces at 1, 2, and 3 σ CL (each differentiated by colors) obtained with 5 years measurement[9] by JUNO. The

[9] To be more precise, we consider the total exposure corresponding to $5 \times 35.8 \times 20 = 3.58 \times 10^3$ kt·GW·yr.

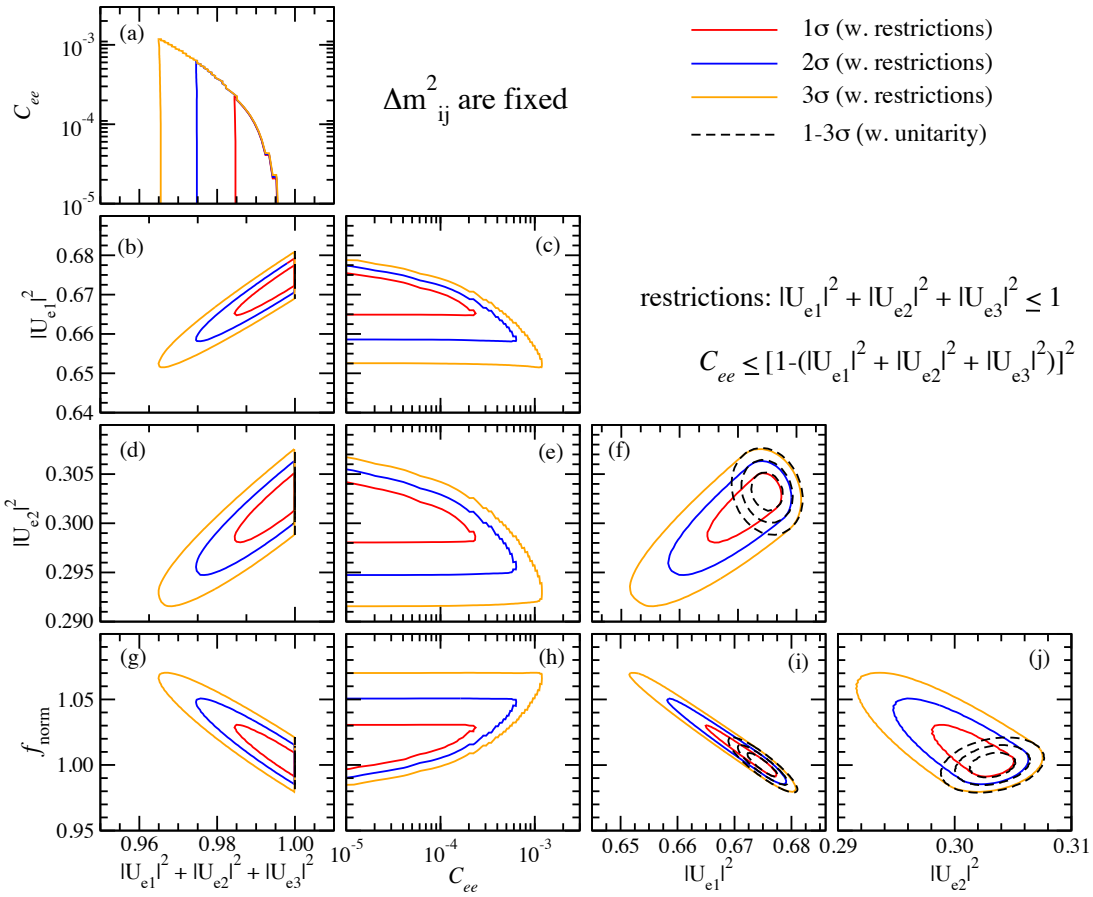

Figure 1: Regions allowed for the five parameters $|U_{e1}|^2$, $|U_{e2}|^2$, $\sum_{i=1}^{3}|U_{ei}|^2$, $\mathcal{C}_{ee}$ and $f_{\rm norm}$, are plotted by projecting into each 2 dimensional subspace at 1σ, 2σ and 3σ CL. The colored solid contours are for the cases with unitarity violation under the conditions $\sum_{i=1}^{3}|U_{ei}|^2 \leq 1$ and $0 \leq \mathcal{C}_{ee} \leq (1-\sum_{i=1}^{3}|U_{ei}|^2)^2$. The black dashed contours are for the standard unitary case.

colored solid contours are for the cases with unitarity violation, while the black dashed contours are for the standard unitary case. Since unitarity is preserved in the true (input) simulated data of JUNO, the contours obtained with ansatz assuming unitarity violation always contain the ones obtained with the standard unitary ansatz.

The first feature we notice is that apparently there is no visible inherent correlation between $\mathcal{C}_{ee}$ and other parameters, including $|U_{e1}|^2+|U_{e2}|^2+|U_{e3}|^2$ and $f_{\rm norm}$, apart from that one side of the boundary has curved shape. We note that the vertical size of the allowed region shown in figure 2(a) is essentially determined by the conditions given in eq. (5.4). It appears that the feature of the boundary may be understood as follows. Although $\mathcal{C}_{ee}$, being of $\mathcal{O}(W^4)$, is tiny and is not so relevant for the oscillation probability, it affects $\sum_i |U_{ei}|^2$ through the unitarity constraint such that $\sum_i |U_{ei}|^2$ decreases as C_{ee} increases, and vice versa.

Of course, there is no counterpart of these contours in the unitary case because $\mathcal{C}_{ee}$

comes as a pure unitarity violating effect in the active three flavor subspace. $\mathcal{C}_{ee}$ is constrained to be small, $\mathcal{C}_{ee} \lesssim 2 \times 10^{-4}$ (10^{-3}) at 1σ (3σ) CL (two degrees of freedom). The stringent constraints obtained for $\mathcal{C}_{ee}$ essentially comes from the upper bound on $\mathcal{C}_{ee}$, eq. (5.4), which is imposed in the analysis. We also note that another measure for unitarity violation $1 - \sum_{i=1}^{3} |U_{ei}|^2$ can be constrained to $1 - \sum_{i=1}^{3} |U_{ei}|^2 \leq 0.01$ (0.03) at 1σ (3σ) CL for one degree of freedom by the JUNO measurement (see table 1 below). The severities of the constraints obtained for $1 - \sum_{i=1}^{3} |U_{ei}|^2$ and $\mathcal{C}_{ee}$ are quite consistent with each other because they are of the order of W^2 and W^4, respectively. It means that it can constrain W matrix elements to the order of $\sim 10\%$.[10]

The accuracy of measurement of $\sin^2\theta_{13}$ in JUNO estimated in [28] is $\simeq 7\%$ level. Then, the natural question would be: Does inclusion of precision data of $\sin^2\theta_{13}$ to be obtained by future measurement by Daya Bay and RENO of $\sim 3\%$ level significantly improve the sensitivity to unitarity violation? We believe that the answer is no. First of all, 7% measurement of $\sin^2\theta_{13}$ implies the accuracy $\delta(\sin^2\theta_{13}) = 1.5 \times 10^{-3}$. It probably means that in our framework the accuracy of measurement of $|U_{e3}|^2$ is $\sim 10^{-3}$, which is an order of magnitude smaller than the 1% level uncertainty of $1 - \sum_{i=1}^{3} |U_{ei}|^2$.

Furthermore, determination of $1 - \sum_{i=1}^{3} |U_{ei}|^2$ is very weakly correlated with $|U_{e3}|^2$. While $|U_{e3}|^2$ is measured by detecting small atmospheric ripples on the long-wavelength solar oscillations, $1 - \sum_{i=1}^{3} |U_{ei}|^2$ is determined in strong correlation with the flux normalization. The flux normalization factor enters into the constant term in the probability in eq. (4.7) with $\alpha = \beta = e$ as

$$f_{\rm norm}(\mathcal{C}_{ee} + \left\{|U_{e1}|^2 + |U_{e2}|^2 + |U_{e3}|^2\right\}^2) \simeq f_{\rm norm}\left\{|U_{e1}|^2 + |U_{e2}|^2 + |U_{e3}|^2\right\}^2, \qquad (5.6)$$

where the approximate equality above is justified because of the smallness of $\mathcal{C}_{ee}$ as seen in figure 1. Then, it is natural to expect that $1 - \sum_{i=1}^{3} |U_{ei}|^2$ would be constrained to the accuracy of $\sim 1 - \sqrt{1 - \sigma_{f_{\rm norm}}} \sim 0.015$, which seems to be consistent with the results presented in figure 1. Therefore, it is important to reduce the flux uncertainty in order to increase the sensitivity to unitarity violation, and improvement of the $|U_{e3}|^2$ measurement would have much less impact on it.

The allowed regions of unitarity violation parameters $\mathcal{C}_{ee}$, and $1 - (|U_{e1}|^2 + |U_{e2}|^2 + |U_{e3}|^2)$, as well as $f_{\rm norm}$, $|U_{e1}|^2$, and $|U_{e2}|^2$ at 1 and 3 σ CL for 1 degree of freedom are summarized in table 1.

5.2.2 Understanding correlations between the parameters

One observes that, except for the ones which involve $\mathcal{C}_{ee}$, the allowed contours in the non-unitary case are much wider and expanded to the particular direction, indicating the correlations between the parameters taken in figure 1. Let us understand this feature. For this purpose we call readers attention to the bottom 4 panels (g), (h), (i), and (j) in figure 1. In the left-bottom panel (g), we see that $|U_{e1}|^2 + |U_{e2}|^2 + |U_{e3}|^2$ is restricted to be unity in the unitary case, as it should. Whereas, when unitarity violation is allowed, the contours are expanded into a left-up direction. The contour cannot expand to the

[10] If all the W matrix elements are equal, it means that $|W| \leq 0.1/\sqrt{N}$.

Table 1: Ranges allowed at 1σ and 3σ CL of five parameters $|U_{e1}|^2$, $|U_{e2}|^2$, $\sum_{i=1}^{3}|U_{ei}|^2$, $\mathcal{C}_{ee}$ and $f_{\rm norm}$, for one degree of freedom.

parameter	1σ range	3σ range
$\|U_{e1}\|^2$	[0.668, 0.676]	[0.654, 0.680]
$\|U_{e2}\|^2$	[0.299, 0.304]	[0.293, 0.307]
$\sum_{i=1}^{3}\|U_{ei}\|^2$	[0.989, 1]	[0.968, 1]
$\mathcal{C}_{ee}$	[0, 10^{-4}]	[0, 10^{-3}]
$f_{\rm norm}$	[0.994, 1.02]	[0.983, 1.063]

right because $|U_{e1}|^2+|U_{e2}|^2+|U_{e3}|^2$ must be equal to or less than unity by $(3+N)$ space unitarity, eq. (4.9). They can extend only to left-up direction because the effect of decrease of $|U_{e1}|^2+|U_{e2}|^2+|U_{e3}|^2$ has to be compensated by increase of the flux normalization $f_{\rm norm}$. It then explains the similar behavior of the contours in the panels (i), and (j).[11]

In the panel (f), when unitarity violation is introduced, the allowed contours prolongate to left-down direction, indicating a positive correlation between $|U_{e1}|^2$ and $|U_{e2}|^2$. If we assume the positive correlation between $|U_{e1}|^2$ and $|U_{e2}|^2$, and taking into account that $|U_{e3}|^2 \ll |U_{e1}|^2, |U_{e2}|^2$, we have the positive correlation between $|U_{e1}|^2$ and $|U_{e1}|^2+|U_{e2}|^2+|U_{e3}|^2$ (between $|U_{e2}|^2$ and $|U_{e1}|^2+|U_{e2}|^2+|U_{e3}|^2$), as indicated in the panel (b) ((d)). It almost completes the discussion to understand the features of correlations between the quantities plotted in figure 1.

Now, what is left is to understand the reason for positive correlation between $|U_{e1}|^2$ and $|U_{e2}|^2$, to which we now turn. In fact, it is quite a nontrivial feature to understand: If we run the same simulation without the constraint (4.11), we have a negative correlation between $|U_{e1}|^2$ and $|U_{e2}|^2$. See figure 2 in appendix B. Here, we focus on the positive correlation between $|U_{e1}|^2$ and $|U_{e2}|^2$ seen in figure 1, and present a model to understand this feature. In appendix B, we will offer the possible explanation of negative correlation between $|U_{e1}|^2$ and $|U_{e2}|^2$ in the case without the constraint.

We have learned from the results of the analysis that $1-\sum_{i=1}^{3}|U_{ei}|^2$ and $\mathcal{C}_{ee}$ are consistently constrained to be small so that $W^2 \lesssim 10^{-2}$. It means that the system is nearly unitary. In the unitary case, it is expected that the JUNO setting has sensitivity to the individual Δm^2_{31} and Δm^2_{32} waves. Let us suppose that this is the case also in the extended parameter space in our $(3+N)$ model. Then, the suitable representation of $P(\bar\nu_e \to \bar\nu_e)$ is given by the non-unitary version of the one derived in ref. [29] ($\alpha = e$ below):

$$P(\bar\nu_\alpha \to \bar\nu_\alpha) = \mathcal{C}_{\alpha\alpha} + \left\{|U_{\alpha1}|^2+|U_{\alpha2}|^2+|U_{\alpha3}|^2\right\}^2 - 4|U_{\alpha1}|^2|U_{\alpha2}|^2\sin^2\frac{\Delta m^2_{21}x}{4E}$$
$$- 2|U_{\alpha3}|^2\left(|U_{\alpha1}|^2+|U_{\alpha2}|^2\right)\left[1-\sqrt{1-4XY\sin^2\frac{\Delta m^2_{21}x}{4E}}\ \cos\left(\frac{\Delta m^2_{\alpha\alpha}x}{2E}\pm\phi^\alpha_\odot\right)\right], \quad (5.7)$$

[11] Later in this section, we offer an alternative but consistent explanation for these features by using a new representation of the $\bar\nu_e$ survival probability, eq. (5.7).

where

$$X \equiv \frac{|U_{\alpha 1}|^2}{|U_{\alpha 1}|^2 + |U_{\alpha 2}|^2}, \qquad Y \equiv \frac{|U_{\alpha 2}|^2}{|U_{\alpha 1}|^2 + |U_{\alpha 2}|^2}, \tag{5.8}$$

and

$$\begin{aligned} \Delta m^2_{\alpha\alpha} &\equiv X|\Delta m^2_{31}| + Y|\Delta m^2_{32}|, \\ \phi^\alpha_\odot &= \arctan\left[(X-Y)\tan\left(\frac{\Delta m^2_{21}x}{4E}\right)\right] - (X-Y)\left(\frac{\Delta m^2_{21}x}{4E}\right). \end{aligned} \tag{5.9}$$

$\phi^\alpha_\odot$ is a slowly varying function of x/E which depends only on the solar parameters, see [29]. The $\pm$ sign in front of $\phi^\alpha_\odot$ determines the mass ordering.

Notice that the function inside the square bracket in (5.7) determines the way how the Δm^2_{31} and Δm^2_{32} waves are superposed, and we assume that the JUNO setting has the sensitivity to it, as was the case of our simple-minded analysis described in section 5.1 used for the unitary case [24]. Then, variations of the parameters must render the fast varying function of x/E inside the square bracket be invariant, at least approximately.

To compute the number of events, the probability in eq. (5.7) should be multiplied by the flux normalization factor $f_{\rm norm}$, as mentioned in the previous section. Then, we must analyze the effective probability defined as $P(\bar\nu_e \to \bar\nu_e)_{\rm eff} \equiv f_{\rm norm} \times P(\bar\nu_e \to \bar\nu_e)$. We now look for the transformations which render $P(\bar\nu_e \to \bar\nu_e)_{\rm eff}$ invariant. They are

$$\begin{aligned} |U_{ei}|^2 &\to \xi |U_{ei}|^2 \quad (i = 1,2,3), \\ f_{\rm norm} &\to \xi^{-2} f_{\rm norm}, \\ \mathcal{C}_{ee} &\to \xi^2 \mathcal{C}_{ee}, \end{aligned} \tag{5.10}$$

where ξ is an arbitrary parameter. Notice that X, Y, Δm^2_{ee}, and $\phi^\alpha_\odot$ are manifestly invariant under (5.10). The invariance of $P(\bar\nu_e \to \bar\nu_e)_{\rm eff}$ under (5.10) implies that the allowed contours can be extended to this "invariance direction". Therefore, $|U_{e1}|^2$ and $|U_{e2}|^2$ must be positively correlated with each other, whereas $|U_{ei}|^2$ $(i = 1, 2)$ and $f_{\rm norm}$ is negatively correlated. The former is consistent with the feature shown in panel (f), and the latter in agreement with the one in panel (g), (i), and (j) in figure 1. Similarly, $\mathcal{C}_{ee}$ must have positive correlation with $|U_{ei}|^2$ and negative correlation with $f_{\rm norm}$, the feature which, however, does not appear to be seen in figure 1. The most important reason for this is $\mathcal{C}_{ee}$ is essentially determined by the conditions given in eq. (5.4), as mentioned earlier.[12]

6 Structure of CP violation in the $(3+N)$ space unitary model

As in the preceding section, we can use the formulas for $P(\nu_\mu \to \nu_e)$ and $P(\nu_\mu \to \nu_\mu)$ given in (4.6) and (4.7) ($\beta = \mu, \alpha = e$ etc.) to do unitarity test in the accelerator neutrino

[12] But, we must note that the validity of the invariance argument is limited. It breaks down at some point because (i) first of all, the invariance (5.10) is broken for χ^2 by the pull term (5.3), and (ii) the variables we are dealing with live only in restricted ranges, either by $(3+N)$ space unitarity, or as a result of fitting the data. Therefore, the scaling argument has its own inherent limitation. For the above mentioned features of correlations which involve $\mathcal{C}_{ee}$, these limitations of our invariance argument may not play a key role, because $\mathcal{C}_{ee}$ is restricted to be very small, $\lesssim 10^{-3}$ (3σ CL).

experiments with muon neutrino beam in near vacuum environment. While we postpone this task to future communications, we want to make remarks on structure of CP violation in the active neutrino sector of our $(3+N)$ unitary model.

The number of CP violating phases in non-unitary $n \times n$ U matrix can be counted by the similar way as in the CKM matrix: It is $2n^2 - n^2 - (2n-1) = (n-1)^2$, in which we have subtracted number of elements $|U_{\alpha i}|$ and number of phases that can be absorbed into the neutrino wave functions. Hence, four phases exist in the U matrix in our $(3+N)$ model ($n=3$), and it can be parameterized, for example, as

$$U = \begin{bmatrix} |U_{e1}| & |U_{e2}| & |U_{e3}|e^{i\phi_1} \\ |U_{\mu 1}|e^{i\phi_2} & |U_{\mu 2}| & |U_{\mu 3}| \\ |U_{\tau 1}|e^{i\phi_3} & |U_{\tau 2}|e^{i\phi_4} & |U_{\tau 3}| \end{bmatrix}. \tag{6.1}$$

Using (4.6) the CP odd combination of the appearance oscillation probabilities is given by

$$\Delta P_{\beta\alpha} \equiv P(\nu_\beta \to \nu_\alpha) - P(\bar{\nu}_\beta \to \bar{\nu}_\alpha) = -4 \sum_{j>i} J_{\alpha\beta ij} \sin\left(\frac{\Delta m^2_{ji} x}{2E}\right) \tag{6.2}$$

where we have defined the generalized Jarlskog invariants [30]

$$J_{\alpha\beta ij} \equiv \mathrm{Im}\left(U_{\alpha i} U^*_{\beta i} U^*_{\alpha j} U_{\beta j}\right). \tag{6.3}$$

They are called "invariants" because they are invariant under phase redefinition of neutrino fields. Though $J_{\alpha\beta ij}$ is unique, up to sign, in unitary case, the property no longer holds in our $(3+N)$ space unitary model. But, some properties remain, e.g., antisymmetry: $J_{\alpha\beta ij} = -J_{\beta\alpha ij}$, $J_{\alpha\beta ij} = -J_{\alpha\beta ji}$. It allows us to show some interesting properties of CP odd combination $\Delta P_{\beta\alpha}$.

Multiplying $U^*_{\alpha j} U_{\beta j}$ to the unitarity relation, the second equation in (4.9),

$$\sum_i U_{\alpha i} U^*_{\beta i} = \delta_{\alpha\beta} - \sum_I W_{\alpha I} W^*_{\beta I} \tag{6.4}$$

and taking imaginary part we obtain the relation

$$\sum_i J_{\alpha\beta ij} = -\mathrm{Im}\left(U^*_{\alpha j} U_{\beta j} W_{\alpha I} W^*_{\beta I}\right) \equiv S_{\alpha\beta j}. \tag{6.5}$$

Because of antisymmetry of $J_{\alpha\beta ij}$ mentioned above we can write $S_{\alpha\beta j}$ as

$$\begin{aligned} S_{\alpha\beta 1} &= J_{\alpha\beta 21} + J_{\alpha\beta 31}, \\ S_{\alpha\beta 2} &= J_{\alpha\beta 12} + J_{\alpha\beta 32}, \\ S_{\alpha\beta 3} &= J_{\alpha\beta 13} + J_{\alpha\beta 23}, \end{aligned} \tag{6.6}$$

from which the relation $S_{\alpha\beta 1} + S_{\alpha\beta 2} + S_{\alpha\beta 3} = 0$ follows. Then, one can easily show that CP odd combination $\Delta P_{\beta\alpha}$ can be written as[13]

$$\Delta P_{\beta\alpha} = -16 J_{\alpha\beta 12} \sin\left(\frac{\Delta m^2_{32} x}{4E}\right) \sin\left(\frac{\Delta m^2_{31} x}{4E}\right) \sin\left(\frac{\Delta m^2_{21} x}{4E}\right) + 4 S_{\alpha\beta 1} \sin\left(\frac{\Delta m^2_{31} x}{2E}\right) + 4 S_{\alpha\beta 2} \sin\left(\frac{\Delta m^2_{32} x}{2E}\right). \tag{6.7}$$

The form of CP-odd combination $\Delta P_{\beta\alpha}$ in (6.7) is interesting because CP violation effect is decomposed into two pieces, one unitary-like x/E dependence (first line), and the other "unitarity-violating" x/E dependence (second line). Of course, the coefficient of the first term receives unitarity violating effect through non-unitary U matrix elements in $J_{\alpha\beta 12}$. But, it should be possible to disentangle between these two different x/E dependences by precision measurement of neutrino spectrum in the next generation experiments [31, 32] provided that the non-unitarity effect is sufficiently large enough. Presence of the second term would provide with us a clear evidence for unitarity violation, because $S_{\alpha\beta i}$ involves explicitly the W matrix elements which bridge between the active to sterile sectors.[14]

To summarize: We have shown in near vacuum environments that the structure of CP odd combination of the appearance oscillation probabilities is illuminating enough to allow us to disentangle unitarity violating piece by studying the x/E dependence of the signal.

7 Unitarity violation in matter: Matter perturbation theory

In this paper we have developed a framework describing unitarity violation at low energies. It utilizes the three active and N sterile neutrino state space which is assumed to be complete, i.e., $(3+N)$ space unitarity. The key issue is whether the model can be formulated in such a way that its prediction is insensitive to the details of the sterile sector, for example, the sterile neutrino mass spectrum. In vacuum we have shown that our $(3+N)$ model satisfies the requirement if $m^2_J \gtrsim 0.1$ eV^2 for $J \geq 4$. An immediate question is if this feature survives in matter. In this section, we investigate this problem in a restricted framework of leading-order matter effect perturbation theory. We will answer the question in the positive but under the additional requirement, eq. (7.17).

We note that our approach which relies on matter perturbation theory is not purely academic. The resultant formulas for the disappearance and appearance probabilities, $P(\nu_\mu \to \nu_\mu)$ and $P(\nu_\mu \to \nu_e)$ to first order in matter perturbation theory, can be utilized in leptonic unitarity test in T2K and T2HK experiments [31, 33]. Notice that keeping higher order terms in W is important because the bound obtainable by the ongoing and

[13] We have used the identity $\sin\left(\frac{\Delta m^2_{32} x}{2E}\right) - \sin\left(\frac{\Delta m^2_{31} x}{2E}\right) + \sin\left(\frac{\Delta m^2_{21} x}{2E}\right) = 4 \sin\left(\frac{\Delta m^2_{32} x}{4E}\right) \sin\left(\frac{\Delta m^2_{31} x}{4E}\right) \sin\left(\frac{\Delta m^2_{21} x}{4E}\right)$. By cyclic permutation one can obtain the other forms with the first coefficient $J_{\alpha\beta 23}$ or $J_{\alpha\beta 31}$.

[14] One must be careful so as not to misinterpret our statement. Through unitarity of $\mathbf{U}$ matrix (4.9), the U matrix always carries information of W matrix. Therefore, CP odd term is not the only place where we see the effect of non-unitarity. But, $\Delta P_{\beta\alpha}$ is special because an explicit W dependent piece may be singled out, as we emphasized above.

the next generation experiments may not be so stringent. Therefore, we do not make any assumptions on the size of W matrix elements in this paper (besides $|W| < 1$).

7.1 Matter perturbation theory of three active plus N sterile unitary system

We formulate the matter perturbation theory of $(3+N)$ space unitary model by assuming that $|A| \ll |\Delta m^2_{31}|$ where $A \equiv 2\sqrt{2}G_F N_e(x)E$, with G_F being the Fermi constant and $N_e(x)$ electron number density in matter, is the Wolfenstein matter potential [34]. In deriving the formulas for the oscillation probabilities, for simplicity, we assume charge-neutrality in matter, and take constant number density approximation for electron, proton and neutron. Inclusion of the spatial dependence can be done assuming adiabaticity, but it will not alter the results in a qualitative way.

To discuss neutrino oscillation in matter in the three active plus N sterile neutrino system the matter potential due to neutral current (NC) as well as charged current (CC) interactions must be taken into account. We therefore take the Hamiltonian in the flavor basis as

$$H = \mathbf{U}\begin{bmatrix} \Delta_1 & 0 & 0 & 0 & 0 & 0 \\ 0 & \Delta_2 & 0 & 0 & 0 & 0 \\ 0 & 0 & \Delta_3 & 0 & 0 & 0 \\ 0 & 0 & 0 & \Delta_4 & 0 & 0 \\ 0 & 0 & 0 & 0 & \cdots & 0 \\ 0 & 0 & 0 & 0 & 0 & \Delta_{3+N} \end{bmatrix}\mathbf{U}^\dagger + \begin{bmatrix} \Delta_A - \Delta_B & 0 & 0 & 0 & 0 & 0 \\ 0 & -\Delta_B & 0 & 0 & 0 & 0 \\ 0 & 0 & -\Delta_B & 0 & 0 & 0 \\ 0 & 0 & 0 & 0 & 0 & 0 \\ 0 & 0 & 0 & 0 & \cdots & 0 \\ 0 & 0 & 0 & 0 & 0 & 0 \end{bmatrix} \tag{7.1}$$

where $\Delta_{i(J)} \equiv \frac{m^2_{i(J)}}{2E}$ as before, as defined in eq. (3.2) and,

$$\Delta_A \equiv \frac{A}{2E}, \qquad \Delta_B \equiv \frac{B}{2E}. \tag{7.2}$$

The matter potentials A and B, which are respectively due to CC and NC interactions, take the forms and the values as

$$\begin{aligned} A &= 2\sqrt{2}G_F N_e E \approx 1.52 \times 10^{-4}\left(\frac{Y_e\rho}{\text{g.cm}^{-3}}\right)\left(\frac{E}{\text{GeV}}\right)\text{eV}^2, \\ B &= \sqrt{2}G_F N_n E = \frac{1}{2}\left(\frac{N_n}{N_e}\right)A, \end{aligned} \tag{7.3}$$

where N_n is the neutron number density in matter.

7.2 Perturbation theory in vacuum mass eigenstate basis

To formulate perturbative treatment it is convenient to work with the vacuum mass eigenstate basis defined as $\tilde{\nu}_a = (\mathbf{U}^\dagger)_{a\beta}\nu_\beta$, in which the Hamiltonian is related to the flavor basis

one as $\tilde{H} \equiv \mathbf{U}^\dagger H \mathbf{U} = \tilde{H}_0 + \tilde{H}_1$, where[15]

$$\tilde{H}_0 = \begin{bmatrix} \Delta_1 & 0 & 0 & 0 & 0 & 0 \\ 0 & \Delta_2 & 0 & 0 & 0 & 0 \\ 0 & 0 & \Delta_3 & 0 & 0 & 0 \\ 0 & 0 & 0 & \Delta_4 & 0 & 0 \\ 0 & 0 & 0 & 0 & \cdots & 0 \\ 0 & 0 & 0 & 0 & 0 & \Delta_{3+N} \end{bmatrix}, \quad \tilde{H}_1 = \mathbf{U}^\dagger \begin{bmatrix} \Delta_A - \Delta_B & 0 & 0 & 0 & 0 & 0 \\ 0 & -\Delta_B & 0 & 0 & 0 & 0 \\ 0 & 0 & -\Delta_B & 0 & 0 & 0 \\ 0 & 0 & 0 & 0 & 0 & 0 \\ 0 & 0 & 0 & 0 & \cdots & 0 \\ 0 & 0 & 0 & 0 & 0 & 0 \end{bmatrix} \mathbf{U}. \quad (7.4)$$

The S matrix in the flavor basis $S(x)$ is related to the one in the vacuum mass eigenstate basis $\tilde{S}(x)$ as

$$S(x) = \mathbf{U}\tilde{S}(x)\mathbf{U}^\dagger \quad (7.5)$$

where

$$\tilde{S}(x) = T\exp\left[-i\int_0^x dx'\tilde{H}(x')\right]. \quad (7.6)$$

We calculate perturbatively the elements of $\tilde{S}$ matrix. Toward the goal, we define $\Omega(x)$ as $\Omega(x) = e^{i\tilde{H}_0 x}\tilde{S}(x)$, which obeys the evolution equation

$$i\frac{d}{dx}\Omega(x) = H_1(x)\Omega(x) \quad (7.7)$$

where

$$H_1(x) \equiv e^{i\tilde{H}_0 x}\tilde{H}_1 e^{-i\tilde{H}_0 x}. \quad (7.8)$$

Then, $\Omega(x)$ can be computed perturbatively as

$$\Omega(x) = 1 + (-i)\int_0^x dx' H_1(x') + (-i)^2\int_0^x dx' H_1(x')\int_0^{x'} dx'' H_1(x'') + \cdots, \quad (7.9)$$

where the "space-ordered" form in (7.9) is essential because of the non-commutativity between $H_1(x)$ of different locations. Having obtained $\Omega(x)$, $\tilde{S}$ matrix can be written as

$$\tilde{S}(x) = e^{-i\tilde{H}_0 x}\Omega(x). \quad (7.10)$$

We calculate $\tilde{S}$ matrix to first order in matter perturbation theory. Since $\tilde{H}_0$ is diagonal, $e^{\pm i\tilde{H}_0 x}$ takes the simple form diag $\left(e^{\pm i\Delta_1 x}, e^{\pm i\Delta_2 x}, e^{\pm i\Delta_3 x}, e^{\pm i\Delta_4 x}, \cdots, e^{\pm i\Delta_{3+N} x}\right)$. Using eqs. (7.8) and (7.9) respectively, we first determine H_1 and then Ω. Using (7.5), the S matrix elements are given by the $\tilde{S}$ matrix elements as

$$\begin{aligned} S_{\alpha\beta} = &\sum_i U_{\alpha i}U^*_{\beta i}\tilde{S}_{ii} + \sum_{i\neq j} U_{\alpha i}U^*_{\beta j}\tilde{S}_{ij} + \sum_{I,j} W_{\alpha I}U^*_{\beta j}\tilde{S}_{Ij} + \sum_{i,J} U_{\alpha i}W^*_{\beta J}\tilde{S}_{iJ} \\ &+ \sum_I W_{\alpha I}W^*_{\beta I}\tilde{S}_{II} + \sum_{I\neq J} W_{\alpha I}W^*_{\beta J}\tilde{S}_{IJ}, \end{aligned} \quad (7.11)$$

[15] If we choose a different phase convention e.g. $\tilde{H}_1 = \mathbf{U}^\dagger \,\mathrm{diag}(\Delta_A, 0, 0, \Delta_B, ..., \Delta_B)\mathbf{U}$, the S matrix discussed in the following will change but the physical observable (oscillation probability) remains the same, as it must. This is confirmed by an explicit calculation.

where the expressions of $\tilde{S}$ matrix elements are given in appendix C. If we decompose $S_{\alpha\beta}$ to zeroth and the first order terms, $S_{\alpha\beta} = S^{(0)}_{\alpha\beta} + S^{(1)}_{\alpha\beta}$, we obtain

$$S^{(0)}_{\alpha\beta} = \sum_k U_{\alpha k} U^*_{\beta k} e^{-i\Delta_k x} + \sum_K W_{\alpha K} W^*_{\beta K} e^{-i\Delta_K x}, \tag{7.12}$$

which is, of course, identical with (4.3), and

$$\begin{aligned}
S^{(1)}_{\alpha\beta} &= \sum_k U_{\alpha k} U^*_{\beta k} e^{-i\Delta_k x} \left[-i(\Delta_A x)|U_{ek}|^2 + i(\Delta_B x) \sum_\gamma |U_{\gamma k}|^2 \right] \\
&+ \sum_K W_{\alpha K} W^*_{\beta K} e^{-i\Delta_K x} \left[-i(\Delta_A x)|U_{eK}|^2 + i(\Delta_B x) \sum_\gamma |W_{\gamma K}|^2 \right] \\
&+ \sum_{k\neq l} U_{\alpha k} U^*_{\beta l} \left[\Delta_A U^*_{ek} U_{el} - \Delta_B \sum_\gamma U^*_{\gamma k} U_{\gamma l} \right] \frac{e^{-i\Delta_l x} - e^{-i\Delta_k x}}{(\Delta_l - \Delta_k)} \\
&+ \sum_{K,l} W_{\alpha K} U^*_{\beta l} \left[\Delta_A W^*_{eK} U_{el} - \Delta_B \sum_\gamma W^*_{\gamma K} U_{\gamma l} \right] \frac{e^{-i\Delta_l x} - e^{-i\Delta_K x}}{(\Delta_l - \Delta_K)} \\
&+ \sum_{k,L} U_{\alpha k} W^*_{\beta L} \left[\Delta_A U^*_{ek} W_{eL} - \Delta_B \sum_\gamma U^*_{\gamma k} W_{\gamma L} \right] \frac{e^{-i\Delta_L x} - e^{-i\Delta_k x}}{(\Delta_L - \Delta_k)} \\
&+ \sum_{K\neq L} W_{\alpha K} W^*_{\beta L} \left[\Delta_A W^*_{eK} W_{eL} - \Delta_B \sum_\gamma W^*_{\gamma K} W_{\gamma L} \right] \frac{e^{-i\Delta_L x} - e^{-i\Delta_K x}}{(\Delta_L - \Delta_K)}.
\end{aligned} \tag{7.13}$$

The oscillation probabilities $P(\nu_\beta \to \nu_\alpha)$ in the appearance ($\beta \neq \alpha$) and disappearance ($\beta = \alpha$) channels can be computed to first order in matter perturbation theory as

$$P(\nu_\beta \to \nu_\alpha) = \left| S^{(0)}_{\alpha\beta} + S^{(1)}_{\alpha\beta} \right|^2 = \left| S^{(0)}_{\alpha\beta} \right|^2 + 2\mathrm{Re}\left[\left(S^{(0)}_{\alpha\beta} \right)^* S^{(1)}_{\alpha\beta} \right]. \tag{7.14}$$

Since the zeroth order term in $P(\nu_\beta \to \nu_\alpha)$ above is already given as the vacuum term, eq. (4.5), we only compute the first order matter correction terms. The results of $P(\nu_\alpha \to \nu_\alpha)^{(1)}$ and $P(\nu_\beta \to \nu_\alpha)^{(1)}$ are given in appendices D and E, respectively.

7.3 Disappearance channels

For simplicity, we first discuss the oscillation probability in the disappearance channel. Given the zeroth-order term in eq. (4.5), we focus on the first-order term here. We present here $P(\nu_\alpha \to \nu_\alpha)^{(1)}$ after averaging over energy resolution dropping the rapidly oscillating

terms due to the large mass squared differences which involve sterile neutrinos[16],

$$
\begin{aligned}
&P(\nu_\alpha \to \nu_\alpha)^{(1)} = 2\mathrm{Re}\left[\left(S^{(0)}_{\alpha\alpha}\right)^* S^{(1)}_{\alpha\alpha}\right] \\
&= -2\sum_{j\neq k} |U_{\alpha j}|^2 |U_{\alpha k}|^2 \sin(\Delta_k - \Delta_j)x \left[(\Delta_A x)|U_{ek}|^2 - (\Delta_B x)\sum_\gamma |U_{\gamma k}|^2\right] \\
&+ 2\sum_j \sum_{k\neq l} |U_{\alpha j}|^2 \mathrm{Re}\left[\Delta_A U_{\alpha k} U^*_{\alpha l} U^*_{ek} U_{el} - \Delta_B U_{\alpha k} U^*_{\alpha l} \sum_\gamma U^*_{\gamma k} U_{\gamma l}\right] \frac{\cos(\Delta_l - \Delta_j)x - \cos(\Delta_k - \Delta_j)x}{(\Delta_l - \Delta_k)} \\
&+ 2\sum_j \sum_l \sum_K |U_{\alpha j}|^2 \mathrm{Re}\left[\Delta_A W_{\alpha K} U^*_{\alpha l} W^*_{eK} U_{el} - \Delta_B W_{\alpha K} U^*_{\alpha l} \sum_\gamma W^*_{\gamma K} U_{\gamma l}\right] \frac{\cos(\Delta_l - \Delta_j)x}{(\Delta_l - \Delta_K)} \\
&- 2\sum_j \sum_k \sum_L |U_{\alpha j}|^2 \mathrm{Re}\left[\Delta_A U_{\alpha k} W^*_{\alpha L} U^*_{ek} W_{eL} - \Delta_B U_{\alpha k} W^*_{\alpha L} \sum_\gamma U^*_{\gamma k} W_{\gamma L}\right] \frac{\cos(\Delta_k - \Delta_j)x}{(\Delta_L - \Delta_k)}, \qquad (7.16)
\end{aligned}
$$

leaving the full expression before averaging to appendix D.

We find that the last two terms in (7.16) violate our requirement that the oscillation probability in our $(3+N)$ model be insensitive to the spectrum of sterile states unless they are smaller than $\mathcal{C}_{ab} \sim \mathcal{O}(W^4)$ which implies

$$
\frac{|\Delta_A|}{(\Delta_J - \Delta_k)} = \frac{|A|}{\Delta m^2_{Jk}} \ll |W|^2. \qquad (7.17)
$$

A severer restriction is not required because these terms are already suppressed by W^2 apart from the energy denominator. From

$$
\frac{|A|}{\Delta m^2_{Jk}} = 2.13 \times 10^{-3} \left(\frac{\Delta m^2_{Jk}}{0.1\mathrm{eV}^2}\right)^{-1} \left(\frac{\rho}{2.8\,\mathrm{g/cm}^3}\right) \left(\frac{E}{1\ \mathrm{GeV}}\right), \qquad (7.18)
$$

we notice that, unless W^2 is extremely small, $W^2 \lesssim 10^{-2}$, the last two terms in (7.16) can be ignored under the same condition as in vacuum, $\Delta m^2_{Jk} \gtrsim 0.1$ eV^2. If we discuss the region of W^2 which is much smaller, we need to restrict ourselves to the case of higher mass sterile neutrinos. If we treat the regime $W^2 \sim 10^{-3}$ ($W^2 \gtrsim 10^{-n}$), we need to limit to $\Delta m^2_{Jk} \simeq m^2_J \gtrsim 1$ eV^2 ($10^{(n-3)}$ eV^2) to keep our $(3+N)$ space unitary model insensitive to details of the sterile sector.

Assuming the further restriction to the sterile mass spectrum such that condition (7.17)

[16] The averaging out procedure involves not only (3.14) but also

$$
\langle(\Delta_A x)\sin(\Delta_k - \Delta_J)x\rangle \approx \langle(\Delta_A x)\sin(\Delta_K - \Delta_J)x\rangle \approx 0, \qquad (7.15)
$$

and cosine as well. It is justified because the rapidly oscillating sine functions are imposed onto monotonic slowly increasing function of x. This feature arises due to $\frac{|\Delta_A|}{\Delta_J} \approx \frac{|A|}{\Delta m^2_{Jk}} \approx \frac{|A|}{|\Delta m^2_{JK}|} \ll 1$, see eq. (7.18).

is fulfilled, we obtain the final form of the first-order matter correction to $P(\nu_\alpha \to \nu_\alpha)$ as

$$
\begin{aligned}
P(\nu_\alpha \to \nu_\alpha)^{(1)} &= -2\sum_{j\neq k}|U_{\alpha j}|^2|U_{\alpha k}|^2\sin(\Delta_k-\Delta_j)x\left[(\Delta_A x)|U_{ek}|^2-(\Delta_B x)\sum_\gamma|U_{\gamma k}|^2\right] \\
&+ 4\sum_j\sum_{k\neq l}|U_{\alpha j}|^2\mathrm{Re}\left[\Delta_A U_{\alpha k}U^*_{\alpha l}U^*_{ek}U_{el}-\Delta_B U_{\alpha k}U^*_{\alpha l}\sum_\gamma U^*_{\gamma k}U_{\gamma l}\right] \\
&\times\frac{\sin^2\frac{(\Delta_k-\Delta_j)x}{2}-\sin^2\frac{(\Delta_l-\Delta_j)x}{2}}{(\Delta_l-\Delta_k)}.
\end{aligned}
\tag{7.19}
$$

This expression is written in terms of only active space U matrix elements. Therefore, with additional condition on the sterile neutrino mass spectrum given in (7.17), the effect of unitarity violation is only through the non-unitarity U matrix to first order in matter perturbation theory. Thus, we find that the most important modification in the oscillation probability due to non-unitarity is in the vacuum expression in the disappearance channel.

7.4 Appearance channels

Despite the expression of $P(\nu_\beta \to \nu_\alpha)^{(1)}$ given in appendix E is a little cumbersome, it has a simple form after averaging over neutrino energy within the energy resolution and using the condition (7.17):

$$
\begin{aligned}
&P(\nu_\beta \to \nu_\alpha)^{(1)} \\
&= 2\sum_{j\neq k}\left[-\mathrm{Re}\left(U^*_{\alpha j}U_{\beta j}U_{\alpha k}U^*_{\beta k}\right)\sin(\Delta_k-\Delta_j)x+\mathrm{Im}\left(U^*_{\alpha j}U_{\beta j}U_{\alpha k}U^*_{\beta k}\right)\cos(\Delta_k-\Delta_j)x\right] \\
&\times\left[(\Delta_A x)|U_{ek}|^2-(\Delta_B x)\sum_\gamma|U_{\gamma k}|^2\right] \\
&+ 2\sum_j\sum_{k\neq l}\mathrm{Re}\left[\Delta_A U^*_{\alpha j}U_{\beta j}U_{\alpha k}U^*_{\beta l}U^*_{ek}U_{el}-\Delta_B U^*_{\alpha j}U_{\beta j}U_{\alpha k}U^*_{\beta l}\sum_\gamma U^*_{\gamma k}U_{\gamma l}\right] \\
&\times\frac{\cos(\Delta_l-\Delta_j)x-\cos(\Delta_k-\Delta_j)x}{(\Delta_l-\Delta_k)} \\
&+ 2\sum_j\sum_{k\neq l}\mathrm{Im}\left[\Delta_A U^*_{\alpha j}U_{\beta j}U_{\alpha k}U^*_{\beta l}U^*_{ek}U_{el}-\Delta_B U^*_{\alpha j}U_{\beta j}U_{\alpha k}U^*_{\beta l}\sum_\gamma U^*_{\gamma k}U_{\gamma l}\right] \\
&\times\frac{\sin(\Delta_l-\Delta_j)x-\sin(\Delta_k-\Delta_j)x}{(\Delta_l-\Delta_k)}.
\end{aligned}
\tag{7.20}
$$

Again, the survived matter correction terms are written in terms of only active space U matrix elements, leaving the important effect of unitarity violation only in the vacuum term.

The obvious question would be: Do the features obtained in the leading order in matter perturbation theory, in particular, the restriction to the sterile masses (7.17), prevails to higher orders? A tantalizing feature of the sterile mass condition (7.17) is that its fulfillment relies on smallness of $A/\Delta m^2_{Jk}$ in our present discussion. Therefore, better treatment of

the matter effect is necessary to know whether our $(3+N)$ model can be insensitive to details of the sterile sector under reasonably strong matter effect. We hope to return to these questions in the near future.

8 Conclusions

In this paper, we have discussed the relationship between low-scale unitarity violation, the one due to new physics at much lower energies than the electroweak scale, and the conventional high-scale unitarity violation. They include (1) presence (absence) of lepton flavor universality in low-scale (high-scale) unitarity violation, and (2) absence (presence) of zero-distance flavor transition in low-scale (high-scale) unitarity violation. In the case of low-scale unitarity violation, it is likely that extension of low energy lepton sector may enrich the features of neutrino mixing and the effects could be detectable by the precision neutrino oscillation experiments.

To provide a framework for leptonic unitarity test, by embodying such features of low-scale unitarity violation, we have constructed a three-active plus N-sterile neutrino model which is assumed to be unitary in the whole $(3+N)$ dimensional state space. Presence of the sterile sector results in non-unitarity in active three neutrino subspace. Though inside this specific model, we sought the possibility that the framework is nearly model-independent to better serve unitarity test. Namely, we require the prediction of the $(3+N)$ model be insensitive to the properties of the sterile sector, such as the number of states N and detailed features of the mass spectrum. We have shown that restriction to the sterile neutrino masses to $m_J^2 \geq 0.1$ eV^2 $(J \geq 4)$, due to decoherence, is sufficient to achieve the desired properties, under a mild assumption of no accidental degeneracy in the mass spectrum, i.e., $|\Delta m_{Ja}^2| \gg |\Delta m_{31}^2|$, or $\gg \Delta m_{21}^2$ where $J = 4, .., 3+N, a = 1, ..., 3+N$. The characteristic features of unitarity violation, as modelled by our $(3+N)$ space unitary model, are as follows:

- the neutrino oscillation probability contains the constant term $\mathcal{C}_{\alpha\beta}$ in (4.8) ($\alpha \neq \beta$ for appearance channels, and $\alpha = \beta$ for disappearance channels), describing the probability leaking into the sterile subspace.

- the mixing matrix in 3×3 active neutrino subspace is non-unitary.

While the second feature is common to high- and low-scale unitarity violation, the first feature is unique to low-scale unitarity violation. Since probability leaking occurs due to presence of sterile sector which has energies comparable to active neutrinos we suspect that the first feature above is generic in low-scale unitarity violation even outside of our $(3+N)$ model.

In our $(3+N)$ space unitary model, the first observable which signals non-unitarity would be nonzero values of $1 - \sum_{i=1}^{3} |U_{\alpha i}|^2$ $(\alpha = e, \mu, \tau)$ in the disappearance channels, and/or $\left|\sum_{j=1}^{3} U_{\alpha j} U_{\beta j}^*\right|$ in the appearance channels. They are both of the order of W^2, where W is the mixing matrix which connects the active and sterile neutrino subspaces. On the other hand, the probability leaking term $\mathcal{C}_{\alpha\beta}$ (see (4.8)) is of the order of W^4.

To verify low-scale unitarity violation finding a nonzero values of $\mathcal{C}_{\alpha\beta}$ would be enough. But, to prove that unitarity violation occurs in the manner predicted by the $(3+N)$ space unitary model, the consistency between order of magnitudes of $\left|\sum_{j=1}^{3} U_{\alpha j} U_{\beta j}^{*}\right|^2$ and $\mathcal{C}_{\alpha\beta}$ $(\alpha \neq \beta)$ (and the corresponding quantities in the disappearance channels) must be checked.

Thus, we have presented a framework for analysis of unitarity violation in the lepton sector which is suitable for low-scale unitarity violation. To examine how it works we have analyzed a simulated data of medium baseline reactor neutrino experiments prepared by assuming a JUNO-like setting. By analyzing the data with our simple-minded statistical procedure, we have shown that the expected superb performance of JUNO would allow us to constrain unitarity violation and the probability leaking parameters as $1-\sum_{i=1}^{3}|U_{ei}|^2 \leq 0.01(0.03)$ and $\mathcal{C}_{ee} \lesssim 2\times 10^{-4}$ (10^{-3}) at 1σ (3σ) CL (two degrees of freedom), respectively, by its 5 years measurement.

We have also discussed in a qualitative way how to detect unitarity violation in accelerator appearance measurement. Using the antisymmetry property of the generalized Jarlskog invariants we have shown in section 6 that the CP odd combination $P(\nu_\beta \to \nu_\alpha) - P(\bar{\nu}_\beta \to \bar{\nu}_\alpha)$ can be decomposed into the two terms with different x/E dependences. See eq. (6.7). If measurement of neutrino energy spectra is sufficiently accurate it would be possible to single out the explicit W matrix dependent piece, providing with us a clear evidence for unitarity violation.

Finally, we have addressed the question of how inclusion of the matter effect alters the nearly model-independent feature of our $(3+N)$ space unitary model. We have learned that if we discuss the region $W^2 \gtrsim 10^{-2}$ the condition on the sterile neutrino masses $m_J^2 \gtrsim 0.1$ eV^2 needed in vacuum is sufficient, but if we want to treat case of even smaller W^2, $W^2 \gtrsim 10^{-n}$, restriction to sterile masses to $m_J^2 \gtrsim 10^{(n-3)}$ eV^2 is necessary for our $(3+N)$ space unitary model be insensitive to details of the sterile sector. Though our treatment in section 7 is restricted to first order in matter perturbation theory it is perfectly applicable to the analysis for a class of the LBL experiments, for example, T2HK. Clearly the similar discussion must be attempted under environment of larger matter effect that is expected in some of the next generation LBL experiments such as DUNE.

Acknowledgments

One of the authors (H.M.) thanks Renata Zukanovich Funchal for intriguing conversations which for him prepared the cradle of this work. He thanks Instituto de Física, Universidade de São Paulo for the great opportunity of stay under support by Fundação de Amparo à Pesquisa do Estado de São Paulo (FAPESP) with grant number 2015/05208-4. C.S.F. is supported by FAPESP under grants 2013/01792-8 and 2012/10995-7. H.N. was supported by Fundação de Amparo à Pesquisa do Estado do Rio de Janeiro (FAPERJ) and Conselho Nacional de Ciência e Tecnologia (CNPq). H.M. and H.N. thank Masashi Yokoyama and the members of his Group in University of Tokyo for their warm hospitality, where part of this work was carried out.

A Bounds on the probability leaking term by $(3+N)$ space unitarity

Here we would like to derive upper and lower bounds on $\mathcal{C}_{\alpha\beta} \equiv \sum_{J=4}^{3+N} |W_{\alpha J}|^2 |W_{\beta J}|^2$ taking into account the constraint from $(3+N)$ space unitarity. First we have the following identity

$$\begin{aligned}\mathcal{C}_{\alpha\beta} &= \left(\sum_{I=4}^{3+N} |W_{\alpha I}|^2\right)\left(\sum_{J=4}^{3+N} |W_{\beta J}|^2\right) - \sum_{I\neq J} |W_{\alpha I} W_{\beta J}|^2 \\ &= \left(1 - \sum_{i=1}^{3} |U_{\alpha i}|^2\right)\left(1 - \sum_{i=1}^{3} |U_{\beta i}|^2\right) - \sum_{I\neq J} |W_{\alpha I} W_{\beta J}|^2, \end{aligned} \tag{A.1}$$

where in the second line, we have used the unitarity constraint (second relation of (4.9)). Holding the first term fixed, we can maximize (minimize) $C_{\alpha\beta}$ by minimizing (maximizing) the *non-negative* second term. Geometrically, the lengths of vectors $W_\alpha \equiv \{W_{\alpha 1}, ..., W_{\alpha N}\}$ and $W_\beta \equiv \{W_{\beta 1}, ..., W_{\beta N}\}$ in N-vector space are fixed and we are rotating them to find configurations which minimize or maximize $\mathcal{C}_{\alpha\beta}$. The second term is non-negative and its minimum is zero.[17] Hence $\mathcal{C}_{\alpha\beta}$ is bounded from above by

$$\mathcal{C}^{\max}_{\alpha\beta} = \left(1 - \sum_{i=1}^{3} |U_{\alpha i}|^2\right)\left(1 - \sum_{i=1}^{3} |U_{\beta i}|^2\right). \tag{A.2}$$

The maximum of the second term in eq. (A.1) occurs when all the elements of W_α and W_β are respectively equal, $W_{\alpha I} = v$ and $W_{\beta J} \equiv w$:[18]

$$\begin{aligned}\mathcal{C}^{\min}_{\alpha\beta} &= \left(1 - \sum_{i=1}^{3} |U_{\alpha i}|^2\right)\left(1 - \sum_{i=1}^{3} |U_{\beta i}|^2\right) - N(N-1)v^2 w^2 \\ &= \left(1 - \sum_{i=1}^{3} |U_{\alpha i}|^2\right)\left(1 - \sum_{i=1}^{3} |U_{\beta i}|^2\right) - (N-1)\mathcal{C}^{\min}_{\alpha\beta}. \end{aligned} \tag{A.3}$$

The second step above follows from the definition $\mathcal{C}^{\min}_{\alpha\beta} = Nv^2w^2$. Solving for $\mathcal{C}^{\min}_{\alpha\beta}$, we have

$$\mathcal{C}^{\min}_{\alpha\beta} = \frac{1}{N}\left(1 - \sum_{i=1}^{3} |U_{\alpha i}|^2\right)\left(1 - \sum_{i=1}^{3} |U_{\beta i}|^2\right). \tag{A.4}$$

The bound on $\mathcal{C}_{\alpha\alpha}$ follows by the similar treatment.

[17] There is a unique configuration: $W_{\alpha I}, W_{\beta I} \neq 0$ for one and only one I while the rest are zero.

[18] If the readers are not convinced by this argument they can derive the same lower bound (A.4) by using the Lagrange multiplier method in which one considers

$$H \equiv \sum_{J=4}^{3+N} |W_{\alpha J}|^2 |W_{\beta J}|^2 + \eta\left(1 - \sum_{j=1}^{3} |U_{\alpha j}|^2 - \sum_{J=4}^{3+N} |W_{\alpha J}|^2\right) + \xi\left(1 - \sum_{j=1}^{3} |U_{\beta j}|^2 - \sum_{J=4}^{3+N} |W_{\beta J}|^2\right)$$

and minimize H in terms of $|W_{\alpha J}|$, η, and ξ.

B Comparison between the non-unitary constrained and constraint-free cases

We recognized that for better understanding of the correlations between $|U_{e1}|^2$ and $|U_{e2}|^2$, and other features of the contours allowed by JUNO data, it is worthwhile to examine the case with and without the constraint (4.11) and compare the results of both cases.

The resultant contours of such analysis are presented in figure 2. The solid and the dashed contours are the cases with and without constraints (4.11). Of course, the regions outside the solid contours are unphysical in our $(3+N)$ state space unitary model. Yet, comparison between the cases with and without is revealing to understand the features of the contours, as we see below.

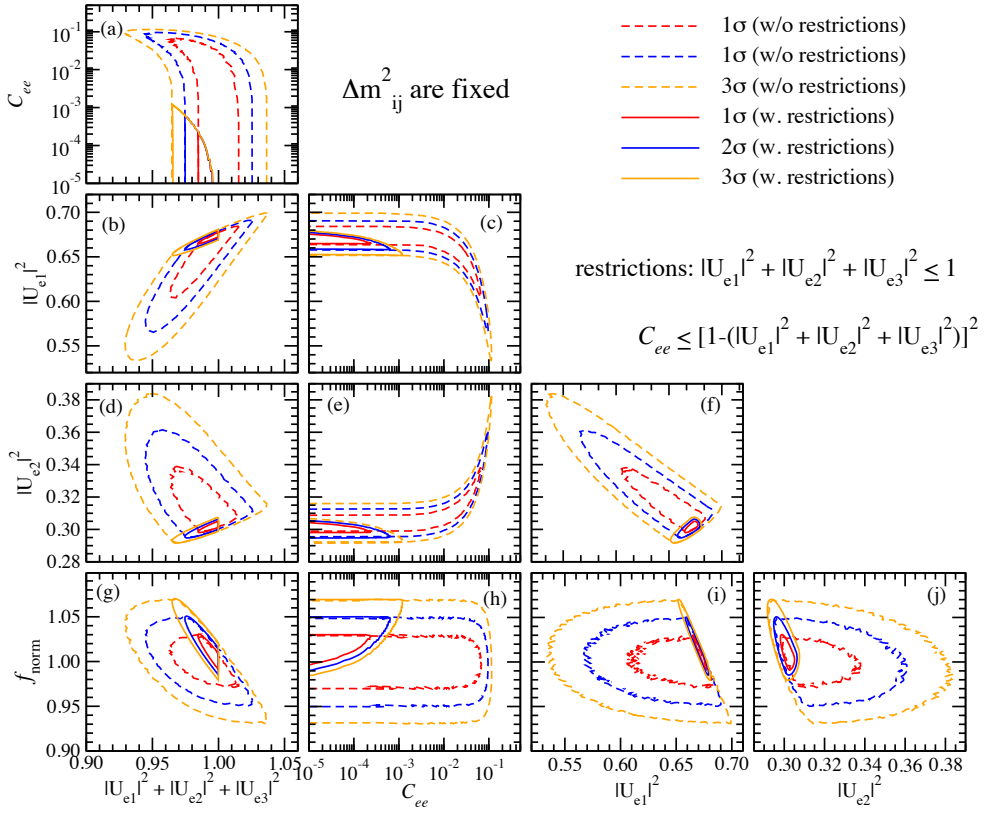

Figure 2: Regions allowed at 1σ, 2σ and 3σ CL of five parameters $|U_{e1}|^2$, $|U_{e2}|^2$, $\sum_{i=1}^{3}|U_{ei}|^2$, $\mathcal{C}_{ee}$ and $f_{\rm norm}$, projected into 2 dimensional subspace. The solid contours are the same as shown in figure 1, that is, the cases with unitarity violation under the conditions $\sum_{i=1}^{3}|U_{ei}|^2 \leq 1$ and $0 \leq \mathcal{C}_{ee} \leq (1-\sum_{i=1}^{3}|U_{ei}|^2)^2$. Whereas the dashed contours correspond also to the cases with unitarity violation but without the above restrictions.

One immediately notices that there exist clear differences between the allowed contours obtained with and without constraints, both in size of the contours and the characteristic features of correlations. In particular, the features of correlations between $|U_{e1}|^2$ and $|U_{e2}|^2$ are completely different, as seen in the panel (f). That is, while $|U_{e1}|^2$ and $|U_{e2}|^2$ are positively correlated in the case with constraint, they are negatively correlated in the case

without constraint with significantly prolongated contours toward left-up direction. Let us understand the features of the results. See section 5.2.2 for a model that enables us to understand the positive correlation between $|U_{e1}|^2$ and $|U_{e2}|^2$ in the case with constraint (4.11).

It appears to us that the features of the contours without constraint can be understood by the following model. Suppose that Δm^2_{31} and Δm^2_{32} waves cannot be discriminated by the JUNO-like setting.[19] Then, we can make approximation $|\Delta m^2_{31}| \approx |\Delta m^2_{32}| \equiv \Delta m^2_{\rm atm}$, which leads to the $\bar{\nu}_e$ oscillation probability

$$\begin{aligned} P(\bar{\nu}_e \to \bar{\nu}_e) &= \mathcal{C}_{ee} + \left\{|U_{e1}|^2 + |U_{e2}|^2 + |U_{e3}|^2\right\}^2 \\ &- 4|U_{e1}|^2|U_{e2}|^2 \sin^2 \frac{\Delta m^2_{21} x}{4E} - 4\left(|U_{e1}|^2 + |U_{e2}|^2\right)|U_{e3}|^2 \sin^2 \frac{\Delta m^2_{\rm atm} x}{4E}. \end{aligned} \tag{B.1}$$

Again we can consider the effective probability by multiplying the flux normalization factor $f_{\rm norm}$ to the probability as done in section 5.2.2, $P(\bar{\nu}_e \to \bar{\nu}_e)_{\rm eff} \equiv f_{\rm norm} \times P(\bar{\nu}_e \to \bar{\nu}_e)$. If we assume that fit to the data can separate the oscillations of the two different frequencies associated with Δm^2_{21} and $\Delta m^2_{\rm atm}$ as well as the constant term, we can obtain the following three observables, if written with the notations $x = |U_{e1}|^2$, $y = |U_{e2}|^2$, $z = |U_{e3}|^2$,

$$f_{\rm norm}\,[\mathcal{C}_{ee} + (x+y+z)^2], \qquad f_{\rm norm}\,xy, \qquad f_{\rm norm}\,(x+y)z \tag{B.2}$$

in addition to Δm^2_{21} and $\Delta m^2_{\rm atm}$. Clearly, the three observables cannot determine the five parameters, and this is the reason why the size of the allowed regions without restrictions (dashed curves) shown in figure 2 are much larger than those with restrictions (solid curves).

Let us now focus on the problem of the correlations. Unlike in the case discussed in section 5, the presence of the leaking term $\mathcal{C}_{ee}$ without conditions given in eq. (5.4) makes a big difference. First, from figure 2(g) we notice the negative correlation between $f_{\rm norm}$ and $x+y+z$, which is naturally expected to keep the energy independent term constant within some uncertainty. This behavior is qualitatively similar to the case with restrictions shown by the solid curves. The impact of the inclusion of $\mathcal{C}_{ee}$ without restrictions is to enlarge significantly the allowed region but keeping the same qualitative feature of anticorrelation.

One might argue that if $x+y+z$ is decreased, $f_{\rm norm}$ does not necessarily have to be increased since $\mathcal{C}_{ee}$ can be increased such that the energy independent term (the first quantity given in (B.2)) kept constant, which is true. However, it would not be possible to keep also the coefficients of energy dependent terms (the second and third quantities given in (B.2)) simultaneously constant by increasing $\mathcal{C}_{ee}$ and decreasing $x+y+z$. Therefore, the anticorrelation between $f_{\rm norm}$ and $x+y+z$ is needed even if $\mathcal{C}_{ee}$ can be varied freely.

However, we did not find any significant correlation between $\mathcal{C}_{ee}$ and $f_{\rm norm}$ as we can see in figure 2(h). This is because the parameter $\mathcal{C}_{ee}$ appears only once in the probability as a constant term, completely independent from other terms whereas x, y and z appear also in the third and fourth terms. If $\mathcal{C}_{ee}$ is increased (decreased), $f_{\rm norm}$ does not have to be decreased (increased) because the other parameters x, y and z can be independently adjusted (no restriction for x, y and z) such that the effective probability is kept constant.

[19] Notice that this is a completely different question from whether the JUNO setting can discriminate between Δm^2_{31} and Δm^2_{32} waves in the unitary case.

Let us try to understand also the other correlations among the parameters. In particular, we focus on the ones in the panels (a), (c), (e) and (f) of figure 2. For the sake of discussion let us assume that $f_{\rm norm}$ is fixed to some value, e.g., to unity, as its variation seems to be not essential to understand the correlations we want to discuss below. It may be partly because, among the five parameters, $f_{\rm norm}$ is already restricted by the pull term given in eq. (5.3).

For a given value of $f_{\rm norm}$, if $\mathcal{C}_{ee}$ is increased, $(x+y+z)^2$ must be decreased which can explains the behavior we see in figure 2 (a). In our analysis, the true (input) values of x, y and z (let us denote, respectively as x_0, y_0 and z_0) are set to be, respectively, $x_0 = 0.675$, $y_0 = 0.303$ and $z_0 = 0.0218$. Ignoring the small value of z_0, when $\mathcal{C}_{ee}$ is increased, $x+y$ should be decreased but keeping xy constant. We note that this is possible only if x extends to the region which is smaller than x_0 and simultaneously y extends to the region where its value is larger than y_0,[20] which can explain the behaviors we can see in the panels (c) and (e) of figure 2. By combining the results shown in panels (a), (c) and (e), we can also understand the correlations we see in the panels of (b) and (d). Once we understand the correlations of $\mathcal{C}_{ee} - x$ (negative) and $\mathcal{C}_{ee} - y$ (positive), we can understand why $x = |U_{e1}|^2$ and $y = |U_{e2}|^2$ are anticorrelated to each other as we can see in the panel (f) in figure 2.

C $\tilde{S}$ matrix elements

Here, we present the results of the active-active (ij), active-sterile (iJ), and the sterile-sterile (IJ) space matrix elements of $\tilde{S}$ to first order in matter perturbation theory formulated in section 7. The ii and ij elements are

$$\begin{aligned}
\tilde{S}_{ii} &= e^{-i\Delta_i x}\Omega_{ii} = e^{-i\Delta_i x}\left[1 - i(\Delta_A x)|U_{ei}|^2 + i(\Delta_B x)\sum_\gamma |U_{\gamma i}|^2\right], \\
\tilde{S}_{ij} &= \Delta_A U^*_{ei}U_{ej}\frac{e^{-i\Delta_j x} - e^{-i\Delta_i x}}{(\Delta_j - \Delta_i)} - \Delta_B \sum_\gamma U^*_{\gamma i}U_{\gamma j}\frac{e^{-i\Delta_j x} - e^{-i\Delta_i x}}{(\Delta_j - \Delta_i)} \qquad (i \neq j).
\end{aligned} \tag{C.1}$$

The iJ and Ij elements are

$$\begin{aligned}
\tilde{S}_{iJ} &= \Delta_A U^*_{ei}W_{eJ}\frac{e^{-i\Delta_J x} - e^{-i\Delta_i x}}{(\Delta_J - \Delta_i)} - \Delta_B \sum_\gamma U^*_{\gamma i}W_{\gamma J}\frac{e^{-i\Delta_J x} - e^{-i\Delta_i x}}{(\Delta_J - \Delta_i)}, \\
\tilde{S}_{Ij} &= \Delta_A W^*_{eI}U_{ej}\frac{e^{-i\Delta_j x} - e^{-i\Delta_I x}}{(\Delta_j - \Delta_I)} - \Delta_B \sum_\gamma W^*_{\gamma I}U_{\gamma j}\frac{e^{-i\Delta_j x} - e^{-i\Delta_I x}}{(\Delta_j - \Delta_I)}.
\end{aligned} \tag{C.2}$$

[20] One might wonder why the other possibility, increasing and decreasing, respectively, x_0 and y_0, does not work. The reason is as follows. Suppose that x and y are varied as $x_0 \to rx_0$ and $y_0 \to y_0/r$ such that xy kept constant. Then, if $\mathcal{C}_{ee}$ is increased, we need $rx_0 + y_0/r < x_0 + y_0$, which implies $r < 1$ for $x_0 > y_0$.

In sterile-sterile subspace, $\tilde{S}$ matrix is given by

$$\tilde{S}_{II} = e^{-i\Delta_I x}\left[1 - i(\Delta_A x)|U_{eI}|^2 + i(\Delta_B x)\sum_\gamma |W_{\gamma I}|^2\right],$$
$$\tilde{S}_{IJ} = \Delta_A W^*_{eI} W_{eJ}\frac{e^{-i\Delta_J x} - e^{-i\Delta_I x}}{(\Delta_J - \Delta_I)} - \Delta_B \sum_\gamma W^*_{\gamma I} W_{\gamma J}\frac{e^{-i\Delta_J x} - e^{-i\Delta_I x}}{(\Delta_J - \Delta_I)} \quad (I \neq J). \text{(C.3)}$$

D Oscillation probabilities in the disappearance channels

The first-order matter correction in the disappearance oscillation probability $P(\nu_\alpha \to \nu_\alpha)$ is given by (next page)

$$
\begin{aligned}
P(\nu_\alpha \to \nu_\alpha)^{(1)} &= -2\sum_{j\neq k} |U_{\alpha j}|^2 |U_{\alpha k}|^2 \sin(\Delta_k - \Delta_j)x \left[(\Delta_A x)|U_{ek}|^2 - (\Delta_B x)\sum_\gamma |U_{\gamma k}|^2 \right] \\
&- 2\sum_k \sum_J |W_{\alpha J}|^2 |U_{\alpha k}|^2 \sin(\Delta_k - \Delta_J)x \left[(\Delta_A x)|U_{ek}|^2 - (\Delta_B x)\sum_\gamma |U_{\gamma k}|^2 \right] \\
&- 2\sum_j \sum_K |U_{\alpha j}|^2 |W_{\alpha K}|^2 \sin(\Delta_K - \Delta_j)x \left[(\Delta_A x)|W_{eK}|^2 - (\Delta_B x)\sum_\gamma |W_{\gamma K}|^2 \right] \\
&- 2\sum_{J\neq K} |W_{\alpha J}|^2 |W_{\alpha K}|^2 \sin(\Delta_J - \Delta_K)x \left[(\Delta_A x)|W_{eK}|^2 - (\Delta_B x)\sum_\gamma |W_{\gamma K}|^2 \right] \\
&+ 2\sum_j \sum_{k\neq l} |U_{\alpha j}|^2 \mathrm{Re}\left[\Delta_A U_{\alpha k} U^*_{\alpha l} U^*_{ek} U_{el} - \Delta_B U_{\alpha k} U^*_{\alpha l} \sum_\gamma U^*_{\gamma k} U_{\gamma l} \right] \frac{\cos(\Delta_l - \Delta_j)x - \cos(\Delta_k - \Delta_j)x}{(\Delta_l - \Delta_k)} \\
&+ 2\sum_J \sum_{k\neq l} |W_{\alpha J}|^2 \mathrm{Re}\left[\Delta_A U_{\alpha k} U^*_{\alpha l} U^*_{ek} U_{el} - \Delta_B U_{\alpha k} U^*_{\alpha l} \sum_\gamma U^*_{\gamma k} U_{\gamma l} \right] \frac{\cos(\Delta_l - \Delta_J)x - \cos(\Delta_k - \Delta_J)x}{(\Delta_l - \Delta_k)} \\
&+ 2\sum_j \sum_l \sum_K |U_{\alpha j}|^2 \mathrm{Re}\left[\Delta_A W_{\alpha K} U^*_{\alpha l} W^*_{eK} U_{el} - \Delta_B W_{\alpha K} U^*_{\alpha l} \sum_\gamma W^*_{\gamma K} U_{\gamma l} \right] \\
&\times \frac{\cos(\Delta_l - \Delta_j)x - \cos(\Delta_K - \Delta_j)x}{(\Delta_l - \Delta_K)} \\
&+ 2\sum_j \sum_k \sum_L |U_{\alpha j}|^2 \mathrm{Re}\left[\Delta_A U_{\alpha k} W^*_{\alpha L} U^*_{ek} W_{eL} - \Delta_B U_{\alpha k} W^*_{\alpha L} \sum_\gamma U^*_{\gamma k} W_{\gamma L} \right] \\
&\times \frac{\cos(\Delta_L - \Delta_j)x - \cos(\Delta_k - \Delta_j)x}{(\Delta_L - \Delta_k)} \\
&+ 2\sum_J \sum_l \sum_K |W_{\alpha J}|^2 \mathrm{Re}\left[\Delta_A W_{\alpha K} U^*_{\alpha l} W^*_{eK} U_{el} - \Delta_B W_{\alpha K} U^*_{\alpha l} \sum_\gamma W^*_{\gamma K} U_{\gamma l} \right] \\
&\times \frac{\cos(\Delta_l - \Delta_J)x - \cos(\Delta_K - \Delta_J)x}{(\Delta_l - \Delta_K)} \\
&+ 2\sum_J \sum_k \sum_L |W_{\alpha J}|^2 \mathrm{Re}\left[\Delta_A U_{\alpha k} W^*_{\alpha L} U^*_{ek} W_{eL} - \Delta_B U_{\alpha k} W^*_{\alpha L} \sum_\gamma U^*_{\gamma k} W_{\gamma L} \right] \\
&\times \frac{\cos(\Delta_L - \Delta_J)x - \cos(\Delta_k - \Delta_J)x}{(\Delta_L - \Delta_k)} \\
&+ 2\sum_j \sum_{K\neq L} |U_{\alpha j}|^2 \mathrm{Re}\left[\Delta_A W_{\alpha K} W^*_{\alpha L} W^*_{eK} W_{eL} - \Delta_B W_{\alpha K} W^*_{\alpha L} \sum_\gamma W^*_{\gamma K} W_{\gamma L} \right] \\
&\times \frac{\cos(\Delta_L - \Delta_j)x - \cos(\Delta_K - \Delta_j)x}{(\Delta_L - \Delta_K)} \\
&+ 2\sum_J \sum_{K\neq L} |W_{\alpha J}|^2 \mathrm{Re}\left[\Delta_A W_{\alpha K} W^*_{\alpha L} W^*_{eK} W_{eL} - \Delta_B W_{\alpha K} W^*_{\alpha L} \sum_\gamma W^*_{\gamma K} W_{\gamma L} \right] \\
&\times \frac{\cos(\Delta_L - \Delta_J)x - \cos(\Delta_K - \Delta_J)x}{(\Delta_L - \Delta_K)}
\end{aligned}
\tag{D.1}
$$

E Oscillation probabilities in the appearance channels

Here, we give the result of first-order matter correction term in the appearance oscillation probability $P(\nu_\alpha \to \nu_\alpha)$. For bookkeeping purpose we decompose it into the three terms:

$$P(\nu_\beta \to \nu_\alpha)^{(1)} = P(\nu_\beta \to \nu_\alpha)|_{\text{First}} + P(\nu_\beta \to \nu_\alpha)|_{\text{Second}} + P(\nu_\beta \to \nu_\alpha)|_{\text{Third}}. \quad \text{(E.1)}$$

The first term is given by

$$\begin{aligned}
&P(\nu_\beta \to \nu_\alpha)|_{\text{First}} \\
&= 2\sum_{j\neq k} \left[-\text{Re}\left(U^*_{\alpha j}U_{\beta j}U_{\alpha k}U^*_{\beta k}\right)\sin(\Delta_k - \Delta_j)x + \text{Im}\left(U^*_{\alpha j}U_{\beta j}U_{\alpha k}U^*_{\beta k}\right)\cos(\Delta_k - \Delta_j)x\right] \\
&\times \left[(\Delta_A x)|U_{ek}|^2 - (\Delta_B x)\sum_\gamma |U_{\gamma k}|^2\right] \\
&+ 2\sum_{J,k} \left[-\text{Re}\left(W^*_{\alpha J}W_{\beta J}U_{\alpha k}U^*_{\beta k}\right)\sin(\Delta_k - \Delta_J)x + \text{Im}\left(W^*_{\alpha J}W_{\beta J}U_{\alpha k}U^*_{\beta k}\right)\cos(\Delta_k - \Delta_J)x\right] \\
&\times \left[(\Delta_A x)|U_{ek}|^2 - (\Delta_B x)\sum_\gamma |U_{\gamma k}|^2\right] \\
&+ 2\sum_{j,K} \left[-\text{Re}\left(U^*_{\alpha j}U_{\beta j}W_{\alpha K}W^*_{\beta K}\right)\sin(\Delta_K - \Delta_j)x + \text{Im}\left(U^*_{\alpha j}U_{\beta j}W_{\alpha K}W^*_{\beta K}\right)\cos(\Delta_K - \Delta_j)x\right] \\
&\times \left[(\Delta_A x)|W_{eK}|^2 - (\Delta_B x)\sum_\gamma |W_{\gamma K}|^2\right] \\
&+ 2\sum_{J\neq K} \left[-\text{Re}\left(W^*_{\alpha J}W_{\beta J}W_{\alpha K}W^*_{\beta K}\right)\sin(\Delta_K - \Delta_J)x + \text{Im}\left(W^*_{\alpha J}W_{\beta J}W_{\alpha K}W^*_{\beta K}\right)\cos(\Delta_K - \Delta_J)x\right] \\
&\times \left[(\Delta_A x)|W_{eK}|^2 - (\Delta_B x)\sum_\gamma |W_{\gamma K}|^2\right] \qquad \text{(E.2)}
\end{aligned}$$

The second term is given by

$$
\begin{aligned}
& P(\nu_\beta \to \nu_\alpha)|_{\text{Second}} \\
&= 2\sum_j \sum_{k\neq l} \text{Re}\left[\Delta_A U^*_{\alpha j} U_{\beta j} U_{\alpha k} U^*_{\beta l} U^*_{ek} U_{el} - \Delta_B U^*_{\alpha j} U_{\beta j} U_{\alpha k} U^*_{\beta l} \sum_\gamma U^*_{\gamma k} U_{\gamma l}\right] \\
&\times \frac{\cos(\Delta_l - \Delta_j)x - \cos(\Delta_k - \Delta_j)x}{(\Delta_l - \Delta_k)} \\
&+ 2\sum_j \sum_{k\neq l} \text{Im}\left[\Delta_A U^*_{\alpha j} U_{\beta j} U_{\alpha k} U^*_{\beta l} U^*_{ek} U_{el} - \Delta_B U^*_{\alpha j} U_{\beta j} U_{\alpha k} U^*_{\beta l} \sum_\gamma U^*_{\gamma k} U_{\gamma l}\right] \\
&\times \frac{\sin(\Delta_l - \Delta_j)x - \sin(\Delta_k - \Delta_j)x}{(\Delta_l - \Delta_k)} \\
&+ 2\sum_J \sum_{k\neq l} \text{Re}\left[\Delta_A W^*_{\alpha J} W_{\beta J} U_{\alpha k} U^*_{\beta l} U^*_{ek} U_{el} - \Delta_B W^*_{\alpha J} W_{\beta J} U_{\alpha k} U^*_{\beta l} \sum_\gamma U^*_{\gamma k} U_{\gamma l}\right] \\
&\times \frac{\cos(\Delta_l - \Delta_J)x - \cos(\Delta_k - \Delta_J)x}{(\Delta_l - \Delta_k)} \\
&+ 2\sum_J \sum_{k\neq l} \text{Im}\left[\Delta_A W^*_{\alpha J} W_{\beta J} U_{\alpha k} U^*_{\beta l} U^*_{ek} U_{el} - \Delta_B W^*_{\alpha J} W_{\beta J} U_{\alpha k} U^*_{\beta l} \sum_\gamma U^*_{\gamma k} U_{\gamma l}\right] \\
&\times \frac{\sin(\Delta_l - \Delta_J)x - \sin(\Delta_k - \Delta_J)x}{(\Delta_l - \Delta_k)} \\
&+ 2\sum_j \sum_l \sum_K \text{Re}\left[\Delta_A U^*_{\alpha j} U_{\beta j} W_{\alpha K} U^*_{\beta l} W^*_{eK} U_{el} - \Delta_B U^*_{\alpha j} U_{\beta j} W_{\alpha K} U^*_{\beta l} \sum_\gamma W^*_{\gamma K} U_{\gamma l}\right] \\
&\times \frac{\cos(\Delta_l - \Delta_j)x - \cos(\Delta_K - \Delta_j)x}{(\Delta_l - \Delta_K)} \\
&+ 2\sum_j \sum_l \sum_K \text{Im}\left[\Delta_A U^*_{\alpha j} U_{\beta j} W_{\alpha K} U^*_{\beta l} W^*_{eK} U_{el} - \Delta_B U^*_{\alpha j} U_{\beta j} W_{\alpha K} U^*_{\beta l} \sum_\gamma W^*_{\gamma K} U_{\gamma l}\right] \\
&\times \frac{\sin(\Delta_l - \Delta_j)x - \sin(\Delta_K - \Delta_j)x}{(\Delta_l - \Delta_K)} \\
&+ 2\sum_J \sum_l \sum_K \text{Re}\left[\Delta_A W^*_{\alpha J} W_{\beta J} W_{\alpha K} U^*_{\beta l} W^*_{eK} U_{el} - \Delta_B W^*_{\alpha J} W_{\beta J} W_{\alpha K} U^*_{\beta l} \sum_\gamma W^*_{\gamma K} U_{\gamma l}\right] \\
&\times \frac{\cos(\Delta_l - \Delta_J)x - \cos(\Delta_K - \Delta_J)x}{(\Delta_l - \Delta_K)} \\
&+ 2\sum_J \sum_l \sum_K \text{Im}\left[\Delta_A W^*_{\alpha J} W_{\beta J} W_{\alpha K} U^*_{\beta l} W^*_{eK} U_{el} - \Delta_B W^*_{\alpha J} W_{\beta J} W_{\alpha K} U^*_{\beta l} \sum_\gamma W^*_{\gamma K} U_{\gamma l}\right] \\
&\times \frac{\sin(\Delta_l - \Delta_J)x - \sin(\Delta_K - \Delta_J)x}{(\Delta_l - \Delta_K)}
\end{aligned}
\tag{E.3}
$$

The third term is given by

$$
\begin{aligned}
&P(\nu_\beta \to \nu_\alpha)|_{\text{Third}} \\
&= 2\sum_j \sum_k \sum_L \text{Re}\left[\Delta_A U^*_{\alpha j} U_{\beta j} U_{\alpha k} W^*_{\beta L} U^*_{ek} W_{eL} - \Delta_B U^*_{\alpha j} U_{\beta j} U_{\alpha k} W^*_{\beta L} \sum_\gamma U^*_{\gamma k} W_{\gamma L}\right] \\
&\times \frac{\cos(\Delta_L - \Delta_j)x - \cos(\Delta_k - \Delta_j)x}{(\Delta_L - \Delta_k)} \\
&+ 2\sum_j \sum_k \sum_L \text{Im}\left[\Delta_A U^*_{\alpha j} U_{\beta j} U_{\alpha k} W^*_{\beta L} U^*_{ek} W_{eL} - \Delta_B U^*_{\alpha j} U_{\beta j} U_{\alpha k} W^*_{\beta L} \sum_\gamma U^*_{\gamma k} W_{\gamma L}\right] \\
&\times \frac{\sin(\Delta_L - \Delta_j)x - \sin(\Delta_k - \Delta_j)x}{(\Delta_L - \Delta_k)} \\
&+ 2\sum_J \sum_k \sum_L \text{Re}\left[\Delta_A W^*_{\alpha J} W_{\beta J} U_{\alpha k} W^*_{\beta L} U^*_{ek} W_{eL} - \Delta_B W^*_{\alpha J} W_{\beta J} U_{\alpha k} W^*_{\beta L} \sum_\gamma U^*_{\gamma k} W_{\gamma L}\right] \\
&\times \frac{\cos(\Delta_L - \Delta_J)x - \cos(\Delta_k - \Delta_J)x}{(\Delta_L - \Delta_k)} \\
&+ 2\sum_J \sum_k \sum_L \text{Im}\left[\Delta_A W^*_{\alpha J} W_{\beta J} U_{\alpha k} W^*_{\beta L} U^*_{ek} W_{eL} - \Delta_B W^*_{\alpha J} W_{\beta J} U_{\alpha k} W^*_{\beta L} \sum_\gamma U^*_{\gamma k} W_{\gamma L}\right] \\
&\times \frac{\sin(\Delta_L - \Delta_J)x - \sin(\Delta_k - \Delta_J)x}{(\Delta_L - \Delta_k)} \\
&+ 2\sum_j \sum_{K\neq L} \text{Re}\left[\Delta_A U^*_{\alpha j} U_{\beta j} W_{\alpha K} W^*_{\beta L} W^*_{eK} W_{eL} - \Delta_B U^*_{\alpha j} U_{\beta j} W_{\alpha K} W^*_{\beta L} \sum_\gamma W^*_{\gamma K} W_{\gamma L}\right] \\
&\times \frac{\cos(\Delta_L - \Delta_j)x - \cos(\Delta_K - \Delta_j)x}{(\Delta_L - \Delta_K)} \\
&+ 2\sum_j \sum_{K\neq L} \text{Im}\left[\Delta_A U^*_{\alpha j} U_{\beta j} W_{\alpha K} W^*_{\beta L} W^*_{eK} W_{eL} - \Delta_B U^*_{\alpha j} U_{\beta j} W_{\alpha K} W^*_{\beta L} \sum_\gamma W^*_{\gamma K} W_{\gamma L}\right] \\
&\times \frac{\sin(\Delta_L - \Delta_j)x - \sin(\Delta_K - \Delta_j)x}{(\Delta_L - \Delta_K)} \\
&+ 2\sum_J \sum_{K\neq L} \text{Re}\left[\Delta_A W^*_{\alpha J} W_{\beta J} W_{\alpha K} W^*_{\beta L} W^*_{eK} W_{eL} - \Delta_B W^*_{\alpha J} W_{\beta J} W_{\alpha K} W^*_{\beta L} \sum_\gamma W^*_{\gamma K} W_{\gamma L}\right] \\
&\times \frac{\cos(\Delta_L - \Delta_J)x - \cos(\Delta_K - \Delta_J)x}{(\Delta_L - \Delta_K)} \\
&+ 2\sum_J \sum_{K\neq L} \text{Im}\left[\Delta_A W^*_{\alpha J} W_{\beta J} W_{\alpha K} W^*_{\beta L} W^*_{eK} W_{eL} - \Delta_B W^*_{\alpha J} W_{\beta J} W_{\alpha K} W^*_{\beta L} \sum_\gamma W^*_{\gamma K} W_{\gamma L}\right] \\
&\times \frac{\sin(\Delta_L - \Delta_J)x - \sin(\Delta_K - \Delta_J)x}{(\Delta_L - \Delta_K)}
\end{aligned}
\tag{E.4}
$$

F Number of events for the JUNO-like setting

We compute the distribution of the number of events coming from the inverse β-decay (IBD) reaction, $\bar{\nu}_e + p \to e^+ + n$, as a function of the visible energy by performing the following integral,

$$\frac{dN(E_{\rm vis})}{dE_{\rm vis}} = n_p t_{\rm exp} \int_{m_e}^{\infty} dE_e \int_{E_{\rm min}}^{\infty} dE \sum_{i={\rm reac}} \frac{d\phi_i(E)}{dE} \epsilon_{\rm det}(E_e) \frac{d\sigma(E, E_e)}{dE_e} \times P_i(\bar{\nu}_e \to \bar{\nu}_e; L_i, E) R(E_e, E_{\rm vis}), \tag{F.1}$$

where n_p is the number of target (free protons), assumed to be $\sim 1.44 \times 10^{33}$ for 20 kt (assuming a similar proton fraction $\simeq 12\%$ as in the case of the Daya Bay detectors [35]), $t_{\rm exp}$ is the exposure, $\epsilon_{\rm det}$ is the detection efficiency assumed to be 100% for simplicity, $d\phi_i(E)/dE$ is the differential fluxes of reactor neutrinos, $d\sigma(E, E_e)/dE_e$ is the IBD cross section, $P_i(\bar{\nu}_e \to \bar{\nu}_e; L_i, E)$ is the $\bar{\nu}_e$ survival probabilities for a given baseline L_i and neutrino energy E, and $R(E_e, E_{\rm vis})$ is the Gaussian resolution function (see below). We ignore the matter effect and use the probability in vacuum as it is an excellent approximation. We note, however, that it is necessary to take it into account for the precision measurement of the solar parameters, see [28, 36].

As a reasonable approximation for our purpose, we ignore the neutron recoil in the IBD reaction and simply assume that neutrino energy, E, and the positron energy, E_e, is related as $E_e = E - (m_n - m_p) \simeq E - 1.3$ MeV. Due to the finite energy resolution, the event distribution can not be obtained as a function of E_e (true positron energy) but as a function of the reconstructed or so called visible energy, $E_{\rm vis}$, which is approximately related to neutrino energy as $E_{\rm vis} \simeq E - (m_n - m_p) + m_e$, after taking into account the energy resolution (see the text below). Regarding the cross section, $d\sigma(E, E_e)/dE_e$, we use the one found in [37].

The differential flux of reactor neutrino $d\phi(E)/dE$ can be computed as,

$$\frac{d\phi(E)}{dE} = \frac{1}{4\pi L^2} S(E) \frac{P_{\rm th}}{\langle E \rangle}, \tag{F.2}$$

where $P_{\rm th}$ is the thermal power of the reactor, $\langle E \rangle \simeq 210$ MeV is the average energy released by per fission computed by taking into account the ratios of the fuel compositions of the reactor (see below).

We can replace, as a good approximation, the reactor complex consisting of 6 and 4 reactors, respectively, at Yangjiang and Taishan sites by a single reactor with the thermal power of 35.8 GW placed at the baseline $L = 52.5$ km from the JUNO detector. We also include the contributions from the far reactor complexes at Daya Bay (with the baseline of 215 km) and Huizhou (with the baseline of 265 km) sites, which contribute, respectively, about 3% and 2% in terms of the total number of events.

For the reactor spectra $S(E)$, which is nothing but the number of neutrinos being emitted per fission per energy (MeV), we use the convenient analytic expressions found in [38] with the typical fuel compositions of the reactors, ^{235}U: ^{239}Pu: ^{238}U: ^{241}Pu = 0.59:

0.28: 0.07: 0.06. For simplicity, we ignore the contributions for geoneutrinos in this work, as it is not very important for our purpose.

$R(E_e, E_{\rm vis})$ is the function which takes into account the finite energy resolution of the detector and is given by

$$R(E_e, E_{\rm vis}) \equiv \frac{1}{\sqrt{2\pi}\sigma(E_e)} \exp\left[-\frac{1}{2}\left(\frac{E_e + m_e - E_{\rm vis}}{\sigma(E_e)}\right)^2\right] \tag{F.3}$$

where the energy resolution is assumed to be [39],

$$\frac{\sigma(E_e)}{(E_e + m_e)} = \frac{3\%}{\sqrt{(E_e + m_e)/{\rm MeV}}}, \tag{F.4}$$

The expected total number of events at JUNO for the 5 years of exposure with 100% detection efficiency (corresponding to the total exposure of $\simeq 3.6 \times 10^3$ kt·GW·yr) is $\simeq 1.4 \times 10^5$.

References

[1] K. A. Olive *et al.* [Particle Data Group Collaboration], "Review of Particle Physics," Chin. Phys. C **38** (2014) 090001. doi:10.1088/1674-1137/38/9/090001

[2] Y. Farzan and A. Y. Smirnov, "Leptonic unitarity triangle and CP violation," Phys. Rev. D **65** (2002) 113001 doi:10.1103/PhysRevD.65.113001 [hep-ph/0201105].

[3] S. Antusch, C. Biggio, E. Fernandez-Martinez, M. B. Gavela and J. Lopez-Pavon, "Unitarity of the Leptonic Mixing Matrix," JHEP **0610** (2006) 084 doi:10.1088/1126-6708/2006/10/084 [hep-ph/0607020].

[4] F. J. Escrihuela, D. V. Forero, O. G. Miranda, M. Tortola and J. W. F. Valle, "On the description of non-unitary neutrino mixing," Phys. Rev. D **92** (2015) no.5, 053009 doi:10.1103/PhysRevD.92.053009 [arXiv:1503.08879 [hep-ph]].

[5] S. Parke and M. Ross-Lonergan, "Unitarity and the three flavor neutrino mixing matrix," Phys. Rev. D **93** (2016) no.11, 113009 doi:10.1103/PhysRevD.93.113009 [arXiv:1508.05095 [hep-ph]].

[6] Z. z. Xing, "Towards testing the unitarity of the 3X3 lepton flavor mixing matrix in a precision reactor antineutrino oscillation experiment," Phys. Lett. B **718**, 1447 (2013) doi:10.1016/j.physletb.2012.12.062 [arXiv:1210.1523 [hep-ph]].

[7] S. Luo, Int. J. Mod. Phys. A **29**, 1444006 (2014). doi:10.1142/S0217751X14440060

[8] S. Luo, Nucl. Phys. B **899**, 312 (2015) doi:10.1016/j.nuclphysb.2015.08.003 [arXiv:1401.0292 [hep-ph]].

[9] Y. F. Li and S. Luo, Phys. Rev. D **93**, no. 3, 033008 (2016) doi:10.1103/PhysRevD.93.033008 [arXiv:1508.00052 [hep-ph]].

[10] S. Schael *et al.* [ALEPH and DELPHI and L3 and OPAL and SLD and LEP Electroweak Working Group and SLD Electroweak Group and SLD Heavy Flavour Group Collaborations], "Precision electroweak measurements on the Z resonance," Phys. Rept. **427**, 257 (2006) doi:10.1016/j.physrep.2005.12.006 [hep-ex/0509008].

[11] J. M. Conrad, W. C. Louis and M. H. Shaevitz, "The LSND and MiniBooNE Oscillation Searches at High Δm^2," Ann. Rev. Nucl. Part. Sci. **63**, 45 (2013) doi:10.1146/annurev-nucl-102711-094957 [arXiv:1306.6494 [hep-ex]].

[12] J. Kopp, P. A. N. Machado, M. Maltoni and T. Schwetz, "Sterile Neutrino Oscillations: The Global Picture," JHEP **1305** (2013) 050 doi:10.1007/JHEP05(2013)050 [arXiv:1303.3011 [hep-ph]].

[13] P. Minkowski, "$\mu \to e\gamma$ at a Rate of One Out of 10^9 Muon Decays?," Phys. Lett. B **67**, 421 (1977). doi:10.1016/0370-2693(77)90435-X

[14] T. Yanagida, "Horizontal Symmetry And Masses Of Neutrinos," Conf. Proc. C **7902131**, 95 (1979).

[15] M. Gell-Mann, P. Ramond and R. Slansky, "Complex Spinors and Unified Theories," Conf. Proc. C **790927**, 315 (1979) [arXiv:1306.4669 [hep-th]].

[16] R. N. Mohapatra and G. Senjanovic, "Neutrino Masses and Mixings in Gauge Models with Spontaneous Parity Violation," Phys. Rev. D **23**, 165 (1981). doi:10.1103/PhysRevD.23.165

[17] A. de Gouvêa and A. Kobach, "Global Constraints on a Heavy Neutrino," Phys. Rev. D **93** (2016) no.3, 033005 doi:10.1103/PhysRevD.93.033005 [arXiv:1511.00683 [hep-ph]].

[18] C. Giunti and C. W. Kim, "Coherence of neutrino oscillations in the wave packet approach," Phys. Rev. D **58**, 017301 (1998) doi:10.1103/PhysRevD.58.017301 [hep-ph/9711363].

[19] D. Hernandez and A. Y. Smirnov, "Active to sterile neutrino oscillations: Coherence and MINOS results," Phys. Lett. B **706** (2012) 360 doi:10.1016/j.physletb.2011.11.031 [arXiv:1105.5946 [hep-ph]].

[20] E. Akhmedov, D. Hernandez and A. Smirnov, "Neutrino production coherence and oscillation experiments," JHEP **1204**, 052 (2012) doi:10.1007/JHEP04(2012)052 [arXiv:1201.4128 [hep-ph]].

[21] F. An *et al.* [JUNO Collaboration], "Neutrino Physics with JUNO," J. Phys. G **43**, no. 3, 030401 (2016) doi:10.1088/0954-3899/43/3/030401 [arXiv:1507.05613 [physics.ins-det]].

[22] M. Maltoni and T. Schwetz, "Sterile neutrino oscillations after first MiniBooNE results," Phys. Rev. D **76** (2007) 093005 doi:10.1103/PhysRevD.76.093005 [arXiv:0705.0107 [hep-ph]].

[23] X. Qian, C. Zhang, M. Diwan and P. Vogel, "Unitarity Tests of the Neutrino Mixing Matrix," arXiv:1308.5700 [hep-ex].

[24] T. Abrãhao, H. Minakata, H. Nunokawa and A. A. Quiroga, "Constraint on Neutrino Decay with Medium-Baseline Reactor Neutrino Oscillation Experiments," JHEP **1511** (2015) 001 doi:10.1007/JHEP11(2015)001 [arXiv:1506.02314 [hep-ph]].

[25] F. P. An *et al.* [Daya Bay Collaboration], Phys. Rev. Lett. **115** (2015) no.11, 111802 doi:10.1103/PhysRevLett.115.111802 [arXiv:1505.03456 [hep-ex]].

[26] J. H. Choi *et al.* [RENO Collaboration], "Observation of Energy and Baseline Dependent Reactor Antineutrino Disappearance in the RENO Experiment," Phys. Rev. Lett. **116** (2016) no.21, 211801 doi:10.1103/PhysRevLett.116.211801 [arXiv:1511.05849 [hep-ex]].

[27] S. F. Ge, K. Hagiwara, N. Okamura and Y. Takaesu, "Determination of mass hierarchy with medium baseline reactor neutrino experiments," JHEP **1305**, 131 (2013) [arXiv:1210.8141 [hep-ph]].

[28] F. Capozzi, E. Lisi and A. Marrone, "Neutrino mass hierarchy and electron neutrino

oscillation parameters with one hundred thousand reactor events," Phys. Rev. D **89**, 013001 (2014) [arXiv:1309.1638 [hep-ph]].

[29] H. Minakata, H. Nunokawa, S. J. Parke and R. Zukanovich Funchal, "Determination of the neutrino mass hierarchy via the phase of the disappearance oscillation probability with a monochromatic anti-electron-neutrino source," Phys. Rev. D **76** (2007) 053004 Erratum: [Phys. Rev. D **76** (2007) 079901] doi:10.1103/PhysRevD.76.053004, 10.1103/PhysRevD.76.079901 [hep-ph/0701151].

[30] C. Jarlskog, "Commutator of the Quark Mass Matrices in the Standard Electroweak Model and a Measure of Maximal CP Violation," Phys. Rev. Lett. **55** (1985) 1039. doi:10.1103/PhysRevLett.55.1039

[31] K. Abe *et al.* [Hyper-Kamiokande Proto- Collaboration], "Physics potential of a long-baseline neutrino oscillation experiment using a J-PARC neutrino beam and Hyper-Kamiokande," PTEP **2015** (2015) 053C02 doi:10.1093/ptep/ptv061 [arXiv:1502.05199 [hep-ex]].

[32] R. Acciarri *et al.* [DUNE Collaboration], "Long-Baseline Neutrino Facility (LBNF) and Deep Underground Neutrino Experiment (DUNE) : Volume 2: The Physics Program for DUNE at LBNF," arXiv:1512.06148 [physics.ins-det].

[33] K. Abe *et al.* [T2K Collaboration], "The T2K Experiment," Nucl. Instrum. Meth. A **659** (2011) 106 doi:10.1016/j.nima.2011.06.067 [arXiv:1106.1238 [physics.ins-det]].

[34] L. Wolfenstein, "Neutrino Oscillations in Matter," Phys. Rev. D **17** (1978) 2369. doi:10.1103/PhysRevD.17.2369

[35] F. P. An *et al.* [Daya Bay Collaboration], "A side-by-side comparison of Daya Bay antineutrino detectors," Nucl. Instrum. Meth. A **685**, 78 (2012) [arXiv:1202.6181 [physics.ins-det]].

[36] Y. F. Li, Y. Wang and Z. z. Xing, Chin. Phys. C **40**, no. 9, 091001 (2016) doi:10.1088/1674-1137/40/9/091001 [arXiv:1605.00900 [hep-ph]].

[37] A. Strumia and F. Vissani, "Precise quasielastic neutrino/nucleon cross-section," Phys. Lett. B **564** (2003) 42 doi:10.1016/S0370-2693(03)00616-6 [astro-ph/0302055].

[38] T. A. Mueller, D. Lhuillier, M. Fallot, A. Letourneau, S. Cormon, M. Fechner, L. Giot and T. Lasserre *et al.*, "Improved Predictions of Reactor Antineutrino Spectra," Phys. Rev. C **83**, 054615 (2011) [arXiv:1101.2663 [hep-ex]].

[39] Y. F. Li, J. Cao, Y. Wang and L. Zhan, "Unambiguous Determination of the Neutrino Mass Hierarchy Using Reactor Neutrinos," Phys. Rev. D **88**, 013008 (2013) [arXiv:1303.6733 [hep-ex]].